







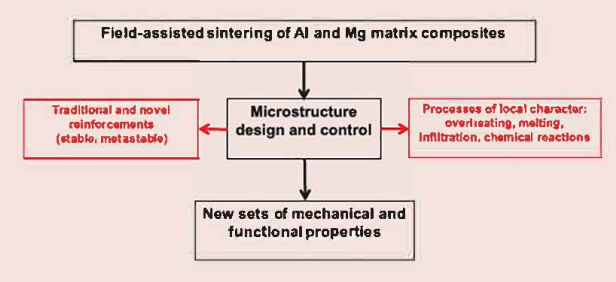
Progress in aluminium and magnesium matrix composites obtained by spark plasma, microwave and induction sintering

Dina V. Dudina^{a,b,c}, Konstantinos Georgarakis^d and Eugene A. Olevsky^e

^aLaboratory of Synthesis of Composite Materials, Lavrentyev Institute of Hydrodynamics SB RAS, Novosibirsk, Russia; ^bLaboratory of Materials Chemistry, Institute of Solid State Chemistry and Mechanochemistry SB RAS, Novosibirsk, Russia; ^cDepartment of Mechanical Engineering, Novosibirsk State Technical University, Novosibirsk, Russia; ^dSchool of Aerospace, Transport and Manufacturing, Cranfield University, Cranfield, UK; ^ePowder Technology Laboratory, San Diego State University, San Diego, CA, USA

ABSTRACT

Aluminium and magnesium matrix composites are attractive lightweight materials with strength surpassing that of the corresponding matrix metals. Recent years have seen extensive research aimed at finding ways to control the structure of metal matrix composites and obtaining materials with new sets of properties. This review aims to show that field-assisted sintering is a promising approach for the powder metallurgy processing of aluminium and magnesium matrix composites. The review focuses on the achievements in the compositional and microstructural design and properties of aluminium and magnesium matrix composites obtained by spark plasma sintering, microwave sintering and induction sintering. Issues related to the process scale-up in the field-assisted sintering technologies are also addressed.



ARTICLE HISTORY

Received 5 December 2020 Accepted 4 May 2022

KEYWORDS

Metal matrix composites; aluminium; magnesium; alloy; spark plasma sintering; induction sintering; microwave sintering

Introduction

The weight of structural elements is an important factor for automotive, aerospace, marine and medical applications. In recent years, extensive research has been conducted to develop materials capable of providing the desired strength while keeping the weight of a structure as low as possible. The innovative car concepts have adopted the multi-material design idea, the essence of which is to use the 'best' material available for each function [1].

Aluminium and magnesium matrix composites are attractive lightweight materials with strength surpassing that of the corresponding matrix metals. The composites can be based not only on aluminium or magnesium matrices but also on Al- and Mg-based alloys. Along with light weight and high strength, the attractive properties of aluminium alloys are high corrosion resistance, good ductility, thermal and electrical conductivity, good machinability and a variety of possible finishes. German [2] marks light metals (titanium, aluminium and magnesium) as one of the future prospects of sintering science and

technology. The powder metallurgy approach is selected to make materials with refined microstructures compared with those produced by ingot metallurgy. The market for sintered aluminium parts has included business machines (with the greatest variety of products), automotive components, aerospace components, power tools, appliances and structural parts. Sintered aluminium-based materials are used for the fabrication of gears, levers, components for office equipment, medical equipment and casings of small electrical motors.

For composites, higher microstructure versatility is a feature of the powder metallurgy processing as compared with casting or infiltration methods. Tailored microstructures often lead to improved mechanical performance and corrosion resistance. In order to be used as structural materials, aluminium alloys should possess strength above 500 MPa at room temperature and tensile elongation of 5% (high-strength alloys) [3]. Sintered aluminium alloy parts can be made competitive with Al-based cast products, Al-based extruded materials and other sintered metallic materials.

Magnesium and its alloys possess attractive properties such as low density, good damping performance, biocompatibility, recyclability and large hydrogen storage capacity, which give them prospects in aerospace, transportation, biomedical and energy sectors [4]. The difficulties that need to be overcome include low strength, insufficient plasticity and low corrosion resistance of magnesium alloys. The application of magnesium alloys is limited by lower ductility and lower mechanical strength as compared with aluminium alloys. Generally, aluminium alloys are less expensive than magnesium alloys [5].

Recent reviews covering certain areas of field-assisted sintering of metal matrix composites (MMCs) indicate a growing interest in the possibilities of scientific and technological upgrades of the conventional processing of these materials [6–10]. The present review aims to highlight the features of field-assisted sintering of lightweight MMCs – composites with Al/Al alloy and Mg/Mg alloy matrices – and mainly covers the literature published in the past decade. The review discusses the principles of the microstructure design, the structure formation and mechanical and functional properties of the Al/Al alloy and Mg/Mg alloy matrix composites obtained by field-assisted techniques – spark plasma, microwave and induction sintering.

Physical principles of spark plasma, microwave and induction sintering and their application to aluminium and magnesium

Spark plasma sintering

Spark plasma sintering (SPS) is a modern sintering technique, in which the sample/tooling assembly is heated by a pulsed direct current [11-19]. The main feature of SPS is the simultaneous application of electric current and uniaxial pressure to the sample (Figure 1). The die and the punches are usually made of graphite, so the electric current passes through the punches and the die and also through the sample in the case of sintering of conductive materials. A historical overview of the development of the field-assisted sintering methods, including SPS, can be found in the monograph [18]. In the SPS, the electric current is applied in the form of pulses, usually 3 ms long. In many laboratory facilities, the pulse sequence is such that 12 pulses are followed by an 'off' period having a duration of two pulses. The voltage in the SPS facilities does not usually exceed 10 V.

Apart from Joule heating, electric-current effects discussed in the context of SPS are electromigration [20], electroplasticity [21] and plasma formation [11]. The electric field effect on mass transport can be taken into account by applying the electromigration

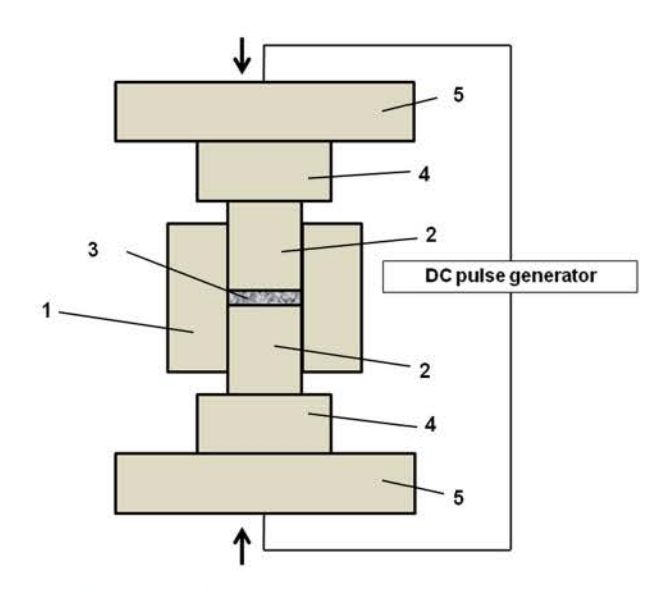


Figure 1. Schematic representation of the tooling/specimen assembly utilized in the SPS processing: (1) graphite die, (2) graphite punches, (3) sample, and (4, 5) graphite spacers.

theory [22]. The flux J_i of the diffusing species can be expressed as

$$J_{i} = -\frac{D_{i}C_{i}}{RT} \left[\frac{RT\partial \ln C_{i}}{\partial x} + Fz^{*}E \right]$$
 (1)

where D_i is the diffusivity of the *i*th species, C_i is the concentration of the species, F is Faraday's constant, z^* is the effective charge on the diffusing species, E is the field strength, R is the gas constant and T is the absolute temperature. Effective charge z^* is a parameter, with which the strength of the electromigration effect is measured. It can be expressed as a sum of z_{wd} , a contribution from the electron wind and z_{el} , an electrostatic component:

$$z^* = z_{wd} + z_{el} \tag{2}$$

In some investigations, the possibility of plasma formation was considered as a mechanism for fast densification of metals and metal-containing mixtures [23,24]. It should be noted that Hulbert et al. [25] found no evidence of the plasma state of matter in the normal SPS runs. However, at voltages higher than those usually used in the SPS furnaces, evaporation of metals and transition of the gaseous phase into an ionized gas is possible, as demonstrated by Saunders et al. [26].

With sintering acceleration observed in the SPS processes relative to conventional sintering and hot pressing, the role of overheating of the inter-particle contacts is of great importance. This question has been studied theoretically and experimentally [27–29]. Kuz'mov et al. [28] showed that the contact temperature may be substantially higher than the average macroscopic temperature of the compact such that melting of the metal can take place in the vicinity of the contact.

An important question for the SPS processing of metallic powders is the possibility of removal/disruption

of oxide films present on the surface of the particles. For oxides that are easily reduced by carbon under conditions of SPS, direct contact with graphite foil or tooling was shown to be critical for surface cleaning and reduction of the oxygen content in the sintered material [30]. For oxides, such as Al₂O₃, which cannot be reduced by carbon at temperatures used for sintering of the metal (Al), a loss of integrity of the oxide film can occur, the concentration of the oxide in the material remaining unchanged. An interesting work was reported by Li et al. [31], who found that the heating rate in the SPS influences the concentration of the oxides in the sintered material. An Al₈₆Ni₆Y_{4.5}Co₂La_{1.5} glassy alloy in the form of powder was subjected to SPS using two different heating rates (5°C min⁻¹ and 40°C min⁻¹). The concentration of oxygen in the material was significantly reduced after SPS conducted at the higher heating rate. Efficient densification of the powder at the higher heating rate was attributed to the removal of the oxide films under the conditions of passing electric current. The evidence of more efficient densification at 40°C min⁻¹ is shown in the corresponding micrographs of the sintered compacts (Figure 2). Xu et al. [32] indicated that a more significant volume expansion of the metal relative to that of the oxide upon heating caused the disruption of Al₂O₃ films facilitating the formation of metallurgical bonds between the Al particles. Melting of aluminium can also contribute to the interparticle bonding quality. The above-described examples show that surface cleaning may play a significant role in the formation of bulk metals during SPS; however, it cannot be regarded as a phenomenon always present in the SPS processing of metallic powders. The possibility of surface cleaning and the underlying physical/ chemical mechanisms of the oxide film removal depend on many factors including the chemical nature of the oxide, the thickness of the film and the crystal structure of the film and its mechanical properties.

Microwave sintering

Microwave sintering uses the energy of a microwave electromagnetic field, which is converted into thermal [33-37]. An important advantage of

microwave heating is volumetric energy absorption in many materials. Since the power generated by the microwave source can be fully converted into thermal energy to heat the sample (without the need to heat the furnace elements), microwave sintering offers much higher heating rates in comparison with conventional processes. While bulk metals are opaque to microwaves, metals in powder form are good microwave absorbers [36,37]. The susceptor material can be used when the powder to be sintered poorly absorbs the microwave radiation. In composite systems, one of the components can play the role of a susceptor.

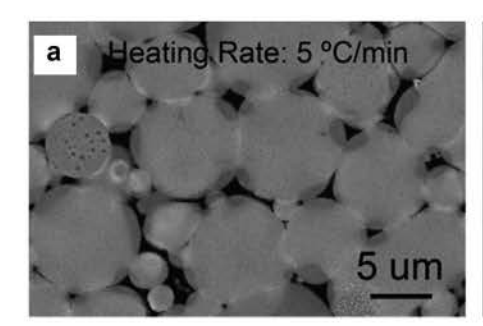
In a microwave sintering set-up (Figure 3), the susceptor material (silicon carbide, SiC) is rapidly heated and provides heat to the specimen. The pre-compacted specimen also absorbs heat. In this manner, hybrid microwave heating occurs ensuring more uniform heating of the specimen and eliminating the disadvantages of conventional heating or heating by microwaves only [38,39]. Due to rapid heating and short cycles, microwave sintering of metal-based compacts can be carried out in air without causing deterioration of the mechanical properties of the sintered materials.

Induction sintering

Induction sintering is based on the use of eddy currents induced in an electrically conductive material [40,41]. The penetration depth of the eddy currents h is determined as

$$h = \frac{1}{\sqrt{\pi f \mu \sigma}},\tag{3}$$

where f is the frequency, μ is the material magnetic permeability and σ is the material electrical conductivity. Induction sintering units are smaller and easier to maintain than conventional sintering furnaces. A conductive container or a die is usually used as a susceptor and is directly heated by the eddy currents (Figure 4). In this case, the powder is heated through radiation and thermal conduction. Alternatively, eddy currents can be induced directly in the pre-



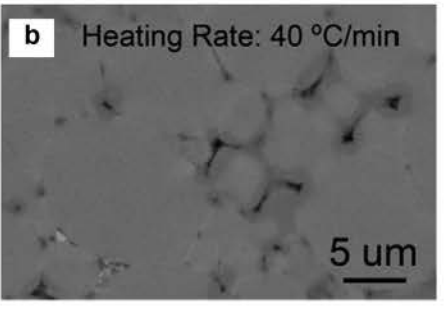


Figure 2. Microstructure of compacts obtained from an Al₈₆Ni₆Y_{4.5}Co₂La_{1.5} glassy powder by SPS at 248.5°C at different heating rates: (a) 5°C min⁻¹ and (b) 40°C min⁻¹. Reprinted from [31], Copyright (2013), with permission from Elsevier.

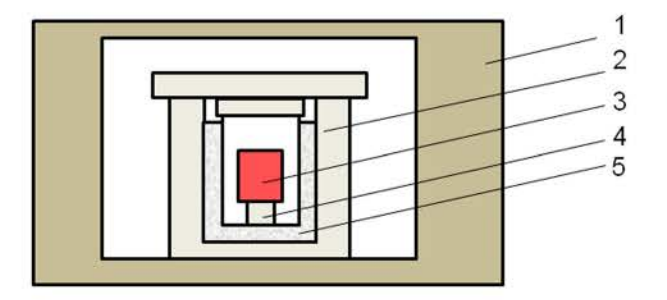


Figure 3. Schematic representation of a microwave sintering set-up: (1) microwave furnace, (2) crucible, (3) specimen, (4) support, and (5) microwave susceptor (SiC powder).

consolidated compacts to be sintered. Both schemes of induction sintering ensure fast heating, reduced sintering times and high energy efficiency.

Field-assisted sintering: advantages over conventional sintering

The advantages of the field-assisted sintering methods over conventional sintering span high heating rates, densification within shorter times and lower energy consumption. For composites, a much wider range of reinforcements is possible, as, by conventional sintering, it may be rather difficult to preserve certain reinforcing phases in the material. The availability of powder consolidation methods capable of preserving the inner structure of the composite particles in terms of phase composition and phase distribution significantly widens the range of achievable properties of the composites. Normally, in the SPS, induction and microwave sintering processes, the major fraction of the material remains in the solid state. Only in the high-temperature regions developing locally, melting of the material can occur. Therefore, the initial microstructure of the powder particles is of importance, as it can, to a great extent, be inherited by the sintered material.

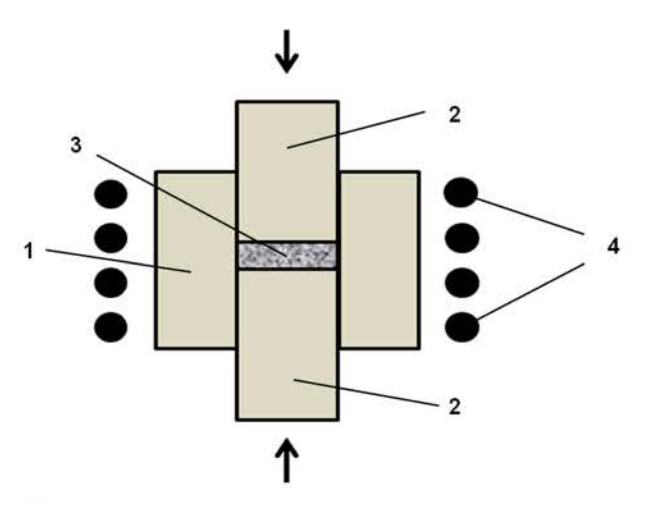


Figure 4. Schematic representation of the susceptor (die)/ specimen assembly in induction sintering: (1) die, (2) punches, (3) sample, and (4) induction coil.

Field-assisted sintering of unreinforced aluminium and magnesium: mechanisms and resulting materials

Investigations of field-assisted sintering of Al and Mg powders shed light on the mass transport mechanisms that operate during the processing of Al- and Mgbased composite mixtures. In this section, the sintering behaviour of Al and Mg powders is discussed. The only reinforcing element in the sintered metals is the oxide phase originating from the native oxide film unavoidable in the commercial and laboratoryproduced powders and powder mixtures.

Olevsky & Froyen developed a constitutive model for SPS that takes into account different transport mechanisms [20]. In that model, the contributions of surface tension, external load and electromigration to shrinkage were jointly analysed. It was found that the electromigration-related material flux can be a significant component of electric current-accelerated diffusion. The model allowed constructing maps of sintering mechanisms operating during SPS. Such a map for an aluminium powder is shown in Figure 5. The map indicates three porosity/grain size domains; in each domain, the applied load, surface tension or electromigration dominates as a driving factor of material transport. The power-law creep induced by an external stress dominates at high porosities. At low porosities, the electromigration can become the dominant mechanism. For small particle sizes and low porosity, the surface tension was found to be the main driving factor for densification. For very small porosities in the electromigration-dominating zone, the elimination of voids may require externally applied loads. The results of modelling agreed

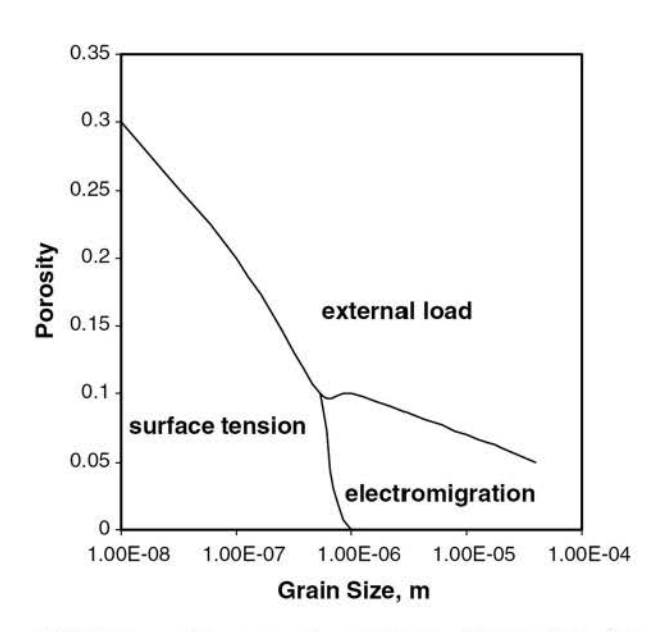


Figure 5. Densification map for aluminium, $U/I = 417 \text{ V m}^{-1}$, T = 673 K, $\bar{\sigma}_x$ = 283 MPa. $\bar{\sigma}_x$ is the effective external stress in xdirection. Reprinted from [20], Copyright (2006), with permission from Elsevier.

satisfactorily with the experimental data on the shrinkage kinetics of aluminium.

According to Xie et al. [42], there are two types of interfaces in aluminium obtained by SPS of a commercially available powder: metal/metal and metal/ oxide/metal. The authors of that work saw the main cause of the destruction of the oxide films present on the surface of the powder in the plastic deformation of the particles of the metal; the deformation was more significant at a higher temperature. In the bulk material obtained by SPS (600°C, 1 h) of a ballmilled Al powder having 38 nm crystallites, a bimodal grain size distribution was observed [43]. An electron backscatter diffraction orientation image map of the sintered aluminium is shown in Figure 6. The authors attributed the presence of large grains to the formation of high-temperature regions in the sample during SPS. Virtually all grain boundaries in the sintered material were of high angle (with misorientations >15°).

During SPS, the response of the inter-particle contacts, Joule heating and plastic deformation may play significant roles varying with the particle size. Cheng et al. [44] found that smaller magnesium particles showed a less significant shape change and a smaller degree of plastic deformation than larger particles. This was explained by the hindering effect of grain boundaries. Thermal softening, localized melting and filling of the pores by the melt were considered as mechanisms contributing to densification.

When a Mg powder was sintered under a pressure of 60 MPa at 525°C-585°C, compacts with relative densities greater than 99% were obtained [23]. Along with grain boundaries, the initial particle boundaries could be observed (Figure 7). It was suggested that the latter were due to oxides still present along the particle boundaries. The boundaries became less visible in samples sintered at higher temperatures. The oxide films remaining in the compacts influenced the fracture behaviour of the material: facets corresponding to the initial Mg powder particles were observed on the fracture surface of the compacts sintered at 525°C.

For aluminium and magnesium, microwave sintering can lead to 82-85% reduction in sintering time and energy savings of 96% compared with conventional sintering [38]. In order to demonstrate the result of the hybrid microwave process in terms of achieving uniform heating, hardness of aluminium and magnesium sintered cylindrical specimens was measured along their radius [38]. The hardness of the hybrid microwave sintered compacts did not change along the radius of the specimen, while the compacts obtained by conventional sintering were softer in the centre.

The possibility of sintering aluminium powders by induction heating was shown in ref. [45]: a mechanically milled aluminium powder was sintered using high-frequency induction heating. The powder was cold-compacted before sintering. The induction sintering process lasted only 3 min and, for

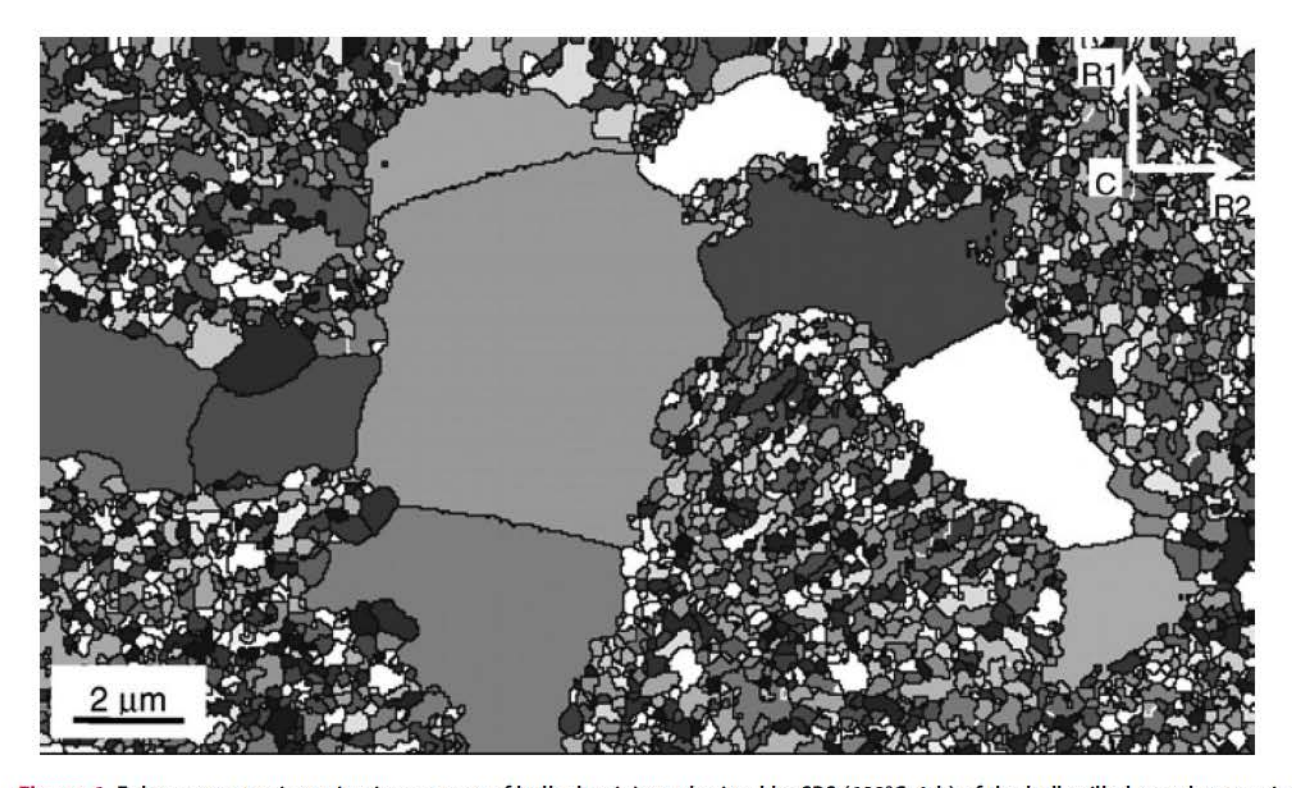
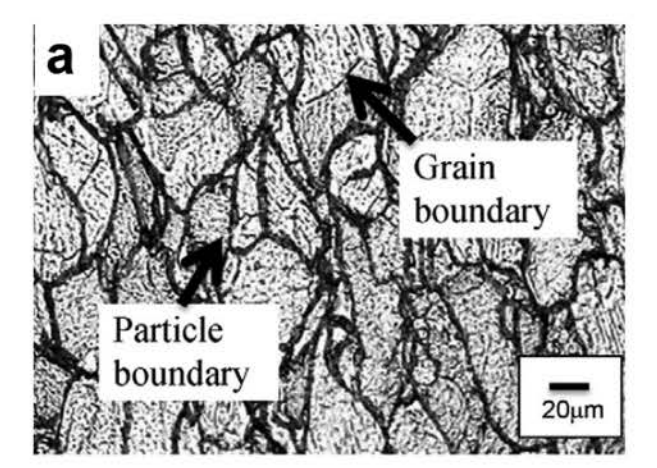


Figure 6. Euler contrast orientation image map of bulk aluminium obtained by SPS (600°C, 1 h) of the ball-milled powder, stearic acid added as a process control agent. Black lines represent misorientations >15°. C represents the compression direction, and R1 and R2 are two orthogonal directions arbitrarily defined in the compression plane. Reprinted from [43], Copyright (2013), with permission from Elsevier.



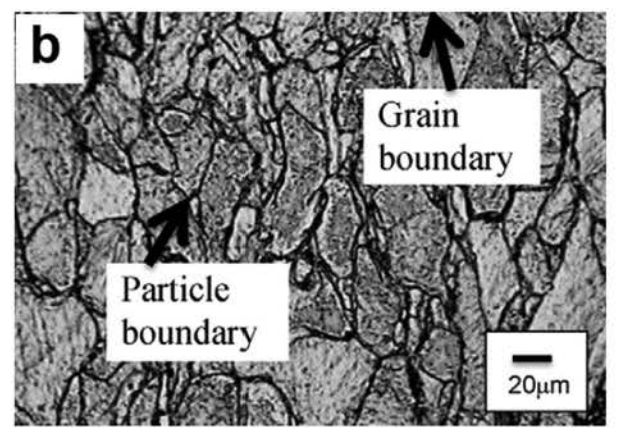


Figure 7. Microstructure of magnesium obtained by SPS, 60 MPa, 5 min: (a) 525°C and (b) 585°C. Reprinted from [23], Copyright (2011), with permission from Elsevier.

simplification, was conducted in air. No new phases were detected in the sintered material, which showed that induction sintering of aluminium is possible in air without any significant oxidation-related effects.

In the processing of composites, the above-mentioned mass transport mechanisms are supplemented by those related to the direct interaction of the reinforcing elements with the electric current/electromagnetic radiation and chemical interactions at the matrix/reinforcement interfaces, as discussed in the following sections.

Recent trends in the selection and design of reinforcements for aluminium and magnesium matrix composites

In this section, traditional and novel reinforcement options for aluminium and magnesium matrix composites are presented. All these reinforcements can be used in composites processed by SPS, induction and microwave sintering. Traditional reinforcements in MMCs are ceramic particles, whiskers and fibres [46]. Sharp corners of the reinforcing elements limit the ductility of these composites [47]. There is a possibility that local overheating can lead to rounding of the sharp corners of the particles of the hard phases

during a field-assisted sintering process. The structure formation of ceramic particle-reinforced aluminium matrix composites obtained by field-assisted sintering is the subject of recent publications [48-58]. Poor wettability between the metal matrix and the ceramic reinforcement leads to the formation of difficult-toeliminate porosity at the interfaces. The porosity can also concentrate within the agglomerates or clusters of the reinforcing particles. Sweet et al. [54] produced aluminium matrix composites reinforced with particles of SiC, AlN or Si₃N₄ by SPS. They found that full densification of composites containing fine ceramic particles was problematic due to the presence of ceramic clusters. The extent, to which aluminium could be forced into those (cluster) regions, determined the residual porosity of the composite. The clusters were, therefore, the principal source of residual porosity of the sintered composites. After sintering at low temperatures, pores were present between the ceramic particles in a cluster, as aluminium did not penetrate the cluster. As the sintering temperature was increased, partial or full penetration of the metal into the clusters was observed.

As seen from examples of ref. [54], ceramic particles in a metal matrix, if clustered, do not sinter with each other under consolidation conditions selected based on the properties of the metal matrix. Those clusters, therefore, comprise a disproportionate part of the total porosity of the composite. In order to fully eliminate the porosity, it is desirable to design composites in such a manner that the particles of the matrix material and those of the reinforcement sinter within the same temperature range. The idea behind the use of metals or metallic alloys as reinforcements is based on the introduction of a harder and stronger metal into matrices of softer metals. In the case of reactive metals, intermetallic layers can form between the particle of the harder metal and the matrix [59,60]. The reinforcement will thus be represented by particles with a core-shell structure.

A rapidly developing trend in the area of MMCs with Al/Al alloy and Mg/Mg alloy matrices is to use metallic glass as a reinforcement. Above their glass transition temperatures, metallic glasses enter a technologically attractive Newtonian flow in the supercooled liquid region ΔT_x between the glass transition temperature T_g and the crystallization temperature T_x . The advantage of metallic glass is its softness and deformability within the supercooled liquid region ΔT_x and its very high strength at ambient temperatures [61]. Similar to oxide glasses, in the supercooled liquid region ΔT_x above T_g , the viscosity of metallic glasses drops drastically and they become liquid-like. Owing to their excellent mechanical properties at room temperature, metallic glasses present a highly promising alternative to ceramic reinforcements, being particularly suitable for strengthening lowmelting temperature metal matrices, such as Al and Mg and their alloys. The composite materials should be designed in such a way that the chosen sintering temperature of the composite powders is within the supercooled liquid region ΔT_x of the glass while being close to the solidus temperature of the matrix alloy. Figure 8 illustrates this approach and schematically shows a drop in the yield stress in metallic glasses and Mg alloys (as possible matrix materials) with the temperature [62]. After compaction to full density and cooling to below T_g and further down to room temperature, the glassy particles become the hard reinforcement phase. Consolidation of the metallic glass-matrix metal (alloy) powder mixtures at temperatures below T_g is also possible, if high pressures are used and a temperature-related viscosity drop of the metallic glass is not necessary for eliminating the porosity.

The limitations imposed by the need to preserve a metastable phase may, in some cases, prevent high-quality sintering of the composite as a whole. As an alternative to metallic glasses, high-entropy alloys [63] are suggested for metal reinforcing purposes. These alloys are thermally stable and possess enhanced mechanical properties relative to conventional alloys. Owing to inherent high hardness and strength [64], quasicrystalline alloys can also be used as reinforcing phases to strengthen softer metallic matrices.

Extensive research has been carried out to find the possibilities of incorporating carbon nanotubes (CNTs) and graphene into Al and Mg matrices [65–68]. The use of hybrid reinforcements (two or more reinforcing phases in the same composite) is justified when each reinforcing phase plays a specific role [69–71]. Kwon et al. [69] obtained aluminium matrix

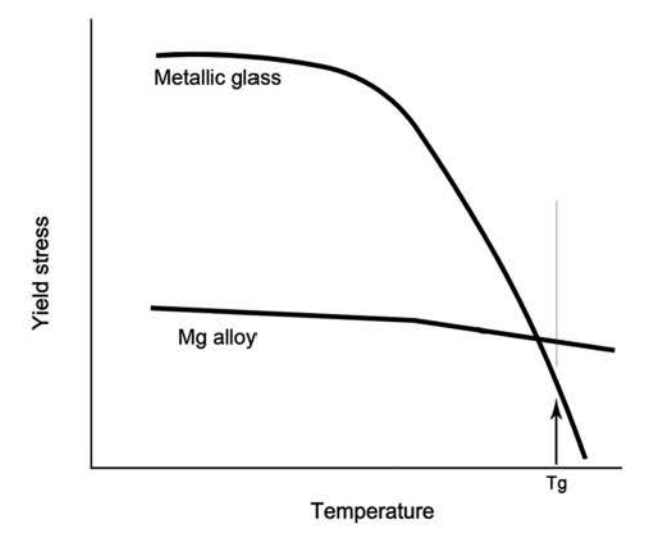


Figure 8. Schematic illustration of the change in the yield stress of a metallic glass and a Mg alloy with increasing temperature. T_g is the glass transition temperature of the metallic glass. Reprinted from [62], Copyright (2009), with permission from Elsevier.

composites reinforced with CNTs and nano-sized SiC particles. The presence of SiC facilitated mixing of aluminium and CNTs during ball milling, so the particles of SiC could be considered as a mixing agent. At the same time, CNTs acted as a lubricant during milling. In the sintered material, particles of SiC reduced the contact area between the Al matrix and CNTs and amount of Al_4C_3 formed at the interface.

Features of the in-situ synthesis of reinforcements during field-assisted sintering

Synthesizing new phases and consolidating the powder within the same field-assisted process offers, along with a technological advantage of reducing the number of processing stages, a possibility of influencing the chemical reactivity of the materials under a specific action of the electric field. Historically designed for solid-state sintering, SPS has emerged into a method of solid-state synthesis under applied electric current and mechanical pressure [72]. SPS dies can be used as chemical reactors for conducting the syntheses of single-phase materials and composites. As, in real SPS processes, the heated and compressed sample is, in most cases, a mixture of powders, an increase in the chemical reactivity under the intrinsic action of electric current is not always easy to quantify. In the reaction mixtures, the contact conditions between the particles of the reactants influence the current density and the temperature in the vicinity of the inter-particle contacts.

During reactive SPS, the Kirkendall effect can cause the formation of pores. Zhang et al. [59] studied the formation mechanism of tungsten aluminides in 80 at.% Al-20 at.% W mixtures subjected to SPS. The aluminium matrix composites were obtained through solid-state diffusion. The particle size of the metallic powders in the initial mixture was found to influence the phase formation and the microstructure of the solid-state sintered material. The reinforcements consisted of W particles surrounded by Al₄W and Al₁₂W, when micrometer-sized particles were used for the synthesis. The material was not well densified owing to the occurrence of the Kirkendall effect.

The sintering time was found to be critical for obtaining materials with improved mechanical strength by reactive SPS. Rodríguez et al. [73] produced aluminium matrix composites by adding small amounts of zirconium to aluminium (0.5, 1 and 1.5 wt.%) and sintering the mixtures by SPS. In order to introduce zirconium into aluminium, a colloidal process based on the use of a zirconium alkoxide was applied. After 3 min of holding the alloy at 625°C during SPS, no intermetallic particles were observed in the microstructure; however, after 1 h, ZrAl₃ platelets nucleated and grew, becoming visible in the

microstructure as inclusions in the Al matrix. Zirconium additions significantly decreased the mechanical strength of the composites relative to pure aluminium when the sintering time was only 3 min. The Zr-containing alloys sintered for 1 h showed higher stiffness and yield strength than the unreinforced aluminium sintered under the same conditions.

In the past decades, microwave energy has been widely used for the synthesis of materials [33], including the synthesis in the combustion mode [34]. The advantage of the energy transfer by means of microwaves over conventional heating is the direct interaction of the electromagnetic waves with the reactants and intensification of the reaction processes. In both processes, heating up to the ignition temperatures is possible without a susceptor. When microwaves are used for the ignition, the target temperature is first reached in the centre of the sample and the combustion front propagates from the centre through the entire volume. After the reaction is complete, the process can continue to sinter the synthesized material into a bulk sample. Induction heating can also be used for the synthesis and ignition of self-propagating high-temperature reactions in powder mixtures [74].

Development of the interfaces between the matrix and the reinforcement in the processes of rapid sintering

Using methods of rapid sintering, it is possible to obtain matrix/reinforcement interfaces formed by interdiffusion across distances of only a few nanometers. A 'non-equilibrium' interface was obtained in aluminium matrix composites reinforced with CNTs [75]. The 'non-equilibrium' term was used to describe an interface that formed prior to crystallization of the carbide, Al₄C₃, layer. The layer containing Al and C was formed between the matrix and CNT due to the interdiffusion of the elements. The formation of amorphous interfacial layers was possible owing to rapid cooling after SPS (at a rate of 500°C min⁻¹). The carbon contained in this layer originated from an amorphous carbon coating on the surface of CNTs formed during the powder processing before sintering. The formation of the 'non-equilibrium' interface allowed improving the tensile properties of the composites.

In order to enable load transfer from an Al matrix to multi-walled CNTs (MWCNTs), certain amounts of Al₄C₃ should be allowed to form [76]. The following aspects of the formation of Al₄C₃ at the interface were highlighted: (1) Al₄C₃ may bridge the outmost and inner walls of the MWCNT preventing peeling of the outmost wall from the inner walls; (2) nanosized Al₄C₃ enhances the interfacial shear resistance between the MWCNTs and the Al matrix, preventing

the pullout of MWCNTs from the matrix. As the concentration of Al₄C₃ is critical, it is important to precisely control the conditions of heat treatment of the composites. In ref. [76], an induction furnace was used to controllably heat-treat composites sintered by SPS.

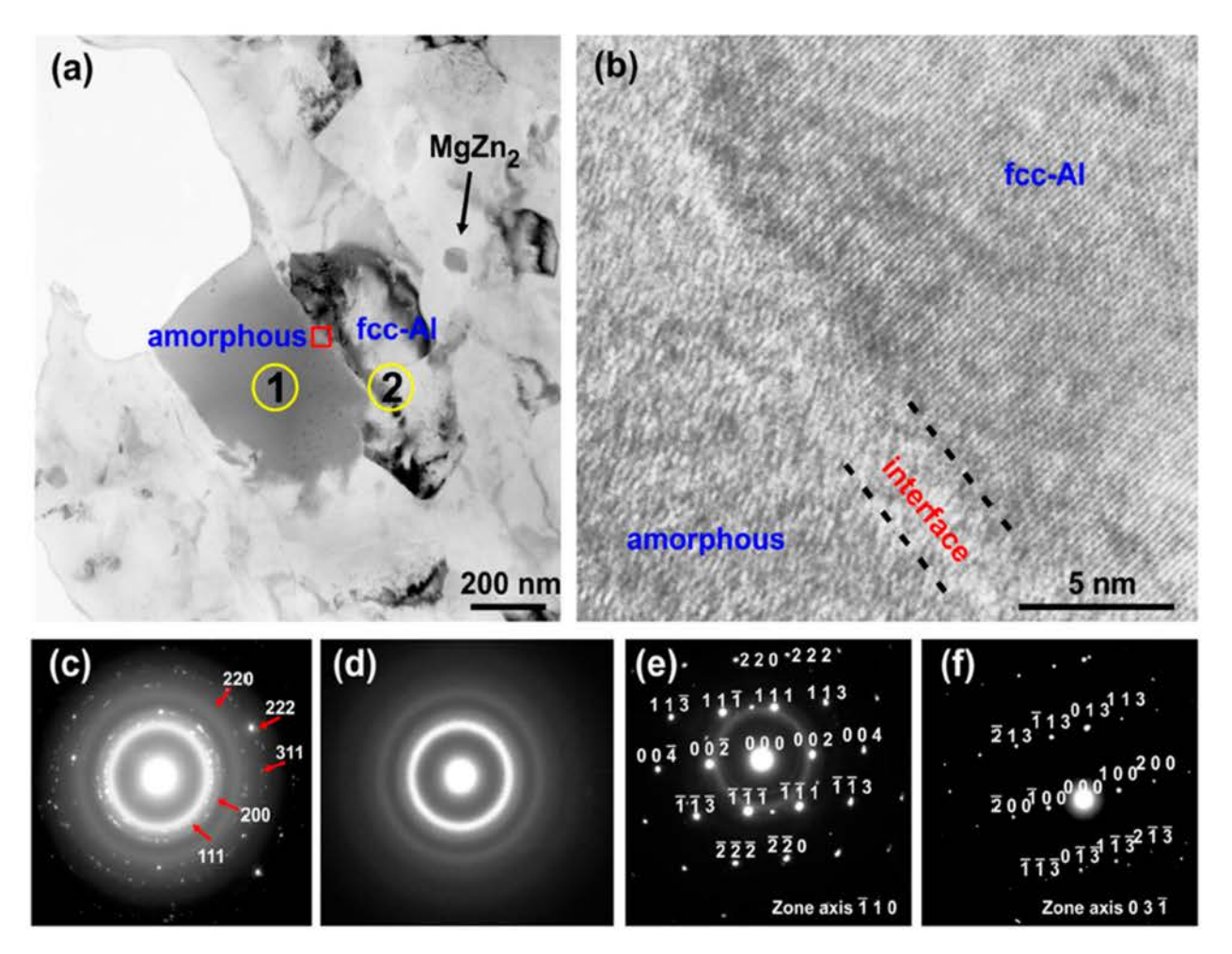
The features of the interfaces developing in Zr₆₅₋ Cu₁₈Ni₇Al₁₀ metallic glass-Al 7075 composite obtained by SPS were studied by Wang et al. [77]. The composite consists of a face-centred cubic (fcc) Al matrix, an amorphous alloy reinforcement and precipitates in the matrix. The selected-area electron diffraction (SAED) pattern of the area corresponding to Figure 9(a) indicates the presence of an amorphous phase and nanocrystalline fcc-Al (Figure 9(c)). SAED patterns taken from area 1 (metallic glass reinforcement), area 2 (fcc-Al) and the MgZn2 precipitate of Figure 9(a) are shown in Figure 9(d-f), respectively. The precipitate was confirmed to be the η-MgZn₂ phase (Figure 9(f)). The interface between the metallic glass and the fcc-Al matrix was observed using hightransmission electron microscopy resolution (HRTEM), as shown in Figure 9(b). A thin layer (thickness of 2-3 nm) was formed at the interface as a result of short to medium range atomic diffusion. This thin interdiffusion layer provided good bonding between the matrix and the reinforcing phase enabling efficient load transfer from the matrix to the reinforcements upon mechanical loading. The limited diffusion between the two phases favoured interfacial bonding and was due to the fast consolidation of the powders at a moderate temperature (SPS at 300°C/600 MPa/ 10 min).

Microstructure formation of aluminium and magnesium matrix composites obtained by field-assisted sintering

Aluminium and magnesium matrix composites obtained by SPS

In this section, examples of the microstructure evolution of aluminium and magnesium matrix composites during SPS are presented and discussed for systems of different compositions. The evidence of local overheating during SPS is also analysed.

An interesting microstructure development was observed during SPS of an Al powder ultrasonically mixed with BN nanoparticles [78]. As seen in Figure 10(a), the agglomerates of BN nanoparticles are located in the spaces between the Al particles after SPS at 600°C for 5 min. When the holding time was increased to 60 min, the BN nanoparticle regions were intermixed with aluminium (Figure 10(b)). Intermixing was attributed to local melting of aluminium at the inter-particle contacts during SPS. The real temperature of the sample was also found



 $\textbf{Figure 9.} \ \, \textbf{TEM/SAED microstructure of } \ \, \textbf{Zr}_{65}\textbf{Cu}_{18}\textbf{Ni}_{7}\textbf{AI}_{10} \ \, \textbf{metallic glass-AI 7075 composite obtained by SPS: (a) bright-field TEM } \\ \textbf{TEM/SAED microstructure of } \ \, \textbf{Zr}_{65}\textbf{Cu}_{18}\textbf{Ni}_{7}\textbf{AI}_{10} \ \, \textbf{metallic glass-AI 7075 composite obtained by SPS: (a) } \\ \textbf{SPS: (a) bright-field TEM } \\ \textbf{SPS: (b) bright-field TEM }$ image, (b) HRTEM image of the interface between the metallic glass and the fcc-Al matrix, (c) SAED of the area corresponding to (a), (d) SAED of area 1 indicating an amorphous structure, (e) SAED of area 2 indicating fcc-Al structure, and (f) SAED of the precipitate phase indicating the η-MgZn₂ structure. Reprinted from [77], Copyright (2016), the article is available under a Creative Commons Attribution 4.0 International License, http://creativecommons.org/licenses/by/4.0/.

to be slightly higher than the measured temperature, as, when aluminium was sintered at a temperature of 620°C measured in the graphite die, molten aluminium was found to squeeze out of the die.

Guan et al. [79] emphasized the importance of controlling the interfacial interactions between the aluminium matrix and the metallic glass reinforcement. By using SPS and hot rolling conducted at a temperature below the crystallization temperature of the metallic glass, it was possible to preserve the cores of the reinforcing particles amorphous with only outer layers crystallized and reacted with aluminium to form FeAl₃ (Figure 11).

During SPS at 550°C, a diffusion layer was formed between CoCrFeMnNi high-entropy alloy particles and the Al 2024 alloy matrix [80]. The layer was serrated on the aluminium alloy side. The authors suggested that this layer formed under conditions of high local temperatures developed during SPS. The hardness of the composite material was found to be higher than that of the aluminium matrix and higher than predicted by the rule of mixtures due to the

presence of the interdiffusion layer and a gradient interface microstructure beneficial for reducing the stress concentration at the interface. Liu et al. [81] showed that, in composites sintered from a mixture of Al and AlCoCrFeNi high-entropy alloy powders, the thickness of the interfacial layer increases with the sintering temperature. This layer has an increased concentration of aluminium relative to the highentropy alloy and presents an Al-based solid solution containing Co, Cr, Fe and Ni. The grains of the transition layer were found to be in the sub-micrometer range, while those of the Al matrix and the highentropy alloy were 20 and 4 µm, respectively. Finer grains of the diffusion layer were explained by the formation of melt upon the passage of current followed by rapid solidification. The authors considered this layer to be favourable for the transition from the isostress to the iso-strain deformation mode of the composite. When the interfacial layer reached a certain thickness (after sintering at 580°C), the hardness of the composite was close to the upper bound calculated from the Voigt model.

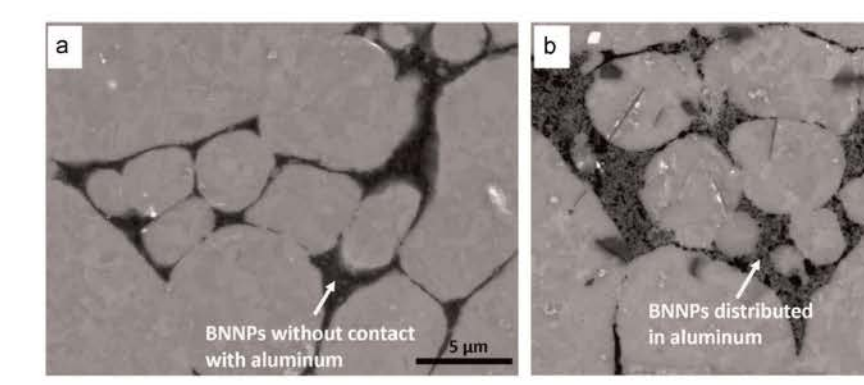


Figure 10. Microstructure of Al-4.5 wt-%BN nanoparticle composites obtained by SPS at 600°C: (a) holding time 5 min and (b) holding time 60 min (back-scattered electron images). Reprinted from [78], Copyright (2015), with permission from Elsevier.

A high-entropy Al_{0.6}CoCrFeNi alloy was used to modify the properties of an amorphous Al₆₅Cu_{16.5-} Ti_{18.5} matrix [82]. The starting high-entropy alloy possessed a single-phase body-centred cubic (bcc) structure. The composite sintered by SPS at 550°C consisted of the bcc phase, fcc phase, AlCu, AlCu₂Ti and an amorphous phase (the sintering temperature was higher than T_x of the initially amorphous matrix alloy powder). The formation of the fcc phase in the composite was attributed to localized high temperatures during sintering, as the consolidation temperature was below the bcc to fcc + bcc transition of the high-entropy alloy. An interdiffusion layer formed between the reinforcing particles and the matrix. The elemental composition of this layer showed that its formation cannot be attributed to (slow) solid/ solid interdiffusion or rapid crystallization of the amorphous matrix. It was, therefore, concluded that this layer formed as a result of enhanced diffusion under the effect of localized high temperatures. The authors proposed a model to calculate the temperature increase ΔT due to the passage of electric current in different regions of the composite structure. It was concluded that the amorphous layer contacting the high-entropy particle was heated more significantly than the particle itself. The sintered composite

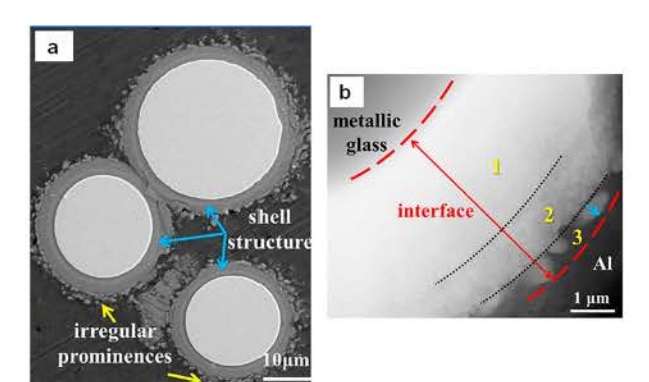


Figure 11. Microstructure of the composite obtained by SPS of 40 vol.-% Fe₅₀Cr₂₅Mo₉C₁₃B₃-Al mixture followed by hot rolling (a) and the structure of the interface (b). Reprinted from [79], Copyright (2019), with permission from Elsevier.

material had a very complex microstructure and exhibited high compressive strength (~3 GPa).

A comparison of results of SPS of Al-Fe₆₆Cr₁₀Nb₅₋ B₁₉ powder mixtures with those of SPS of a pre-compacted pellet of the same composition (compaction pressure 400 MPa) suggested that local heating at the interface caused by interfacial resistance is an important factor influencing the reaction advancement at the interface and the formation of intermetallics [83].

In an investigation of the formation of aluminium matrix composites reinforced with carbon fibres during SPS, Lalet et al. [84] found that the pulse parameters (the number of ON and OFF periods) influenced the interfacial reactions. With the ON/ OFF pulsing ratio set at 24:1, a microstructure similar to that of composites obtained by hot pressing was observed. Under 12:2, 6:4 and 3:3 pulsing patterns, the oxide layer present on aluminium fractured and Al₄C₃ formed at the Al/carbon fibre interface. The direct contact between aluminium and the fibre was explained by the infiltration of molten aluminium through the disrupted Al₂O₃ layer. When the pulsing pattern was such that the ON time was short, a high current had to be applied: at 4:6 pulsing pattern, molten aluminium leaked out of the die, although the temperature measured by the thermocouple (in direct contact with the sample) at that moment was only 500°C. Therefore, the application of a high current led to significant overheating and caused melting of aluminium. The observed crystallization of the initially amorphous Al2O3 layer was also put forward as the evidence of high local temperatures.

Aluminium and magnesium matrix composites obtained by microwave sintering

In composites sintered by microwaves, the presence of a component absorbing microwaves plays an important role in the microstructure formation. The influence of susceptor contained in the composite mixture is discussed below using examples elaborated in refs. [67,85–87]. Silicon carbide SiC is often used as a reinforcement in MMCs sintered by microwaves. Thakur et al. [85] used two-directional (hybrid) microwave sintering to fabricate Al/Ti metastable composites and Al/(Ti+SiC) composites. SiC particles contained in the powder mixtures contributed to the heating process of the compact by acting as a microwave absorbent. CNTs added to a Mg alloy played a dual role of mechanical reinforcement and microwave susceptor [67]. It was found that the interaction between an Al matrix and WC reinforcing particles occurred at lower sample temperatures in microwave sintered composites than in conventionally sintered composites [86]. Microwave heating caused a higher temperature at the interface of Al and WC particles than the macroscopic sample temperature due to the superior absorption of microwaves by the WC particles. The formation of interfaces in Al/(Ti,W)C composites prepared by microwave sintering was studied by Zheng et al. [87]. Microwave sintering at 580°C, which is close to the solidus temperature of Al 6061 alloy, led to the formation of compacts with altered shape because of bubbling and melt squeezing out of the compact. The evidence of local melting of the matrix material was also found in the microstructure of the sample sintered at a lower temperature (560° C): the corners of the (Ti,W)C particles in the sintered material were not as acute as in the raw powder. It was suggested that the presence of a liquid phase between Al and (Ti,W)C was caused by a higher absorbing ability of (Ti,W)C in comparison with the Al alloy and an additional heat transfer to the alloy matrix surrounding the ceramic particles. The ability of the (Ti,W)C particles to absorb the microwave energy could be enhanced by their geometrical characteristics - a small size and the presence of sharp surface features.

Treatment of powders by microwaves can also be used for realizing the combustion synthesis of MMCs. In-situ Al₂O₃- and Al₃Zr-reinforced aluminium matrix composites were obtained by the SiC-assisted combustion synthesis [88]. The reaction mixture was composed of Al and ZrO₂ powders. Aluminium was taken in excess to form both the matrix and the reinforcing phases. The synthesis of the composite occurred via the following reaction:

$$13Al + 3ZrO_2 = 2Al_2O_3 + 3Al_3Zr$$

The heating profiles of Al+ZrO₂ powder mixtures in a SiC susceptor-assisted microwave combustion synthesis process are shown in Figure 12. The reaction mixture with stoichiometry to fully convert aluminium into the ceramic phases (mixture C) shows a very fast temperature rise corresponding to the combustion reaction. In mixtures A and B, due to excess aluminium, the temperatures developed during the synthesis were lower. The microstructure of the composites was found to be finer than that of the

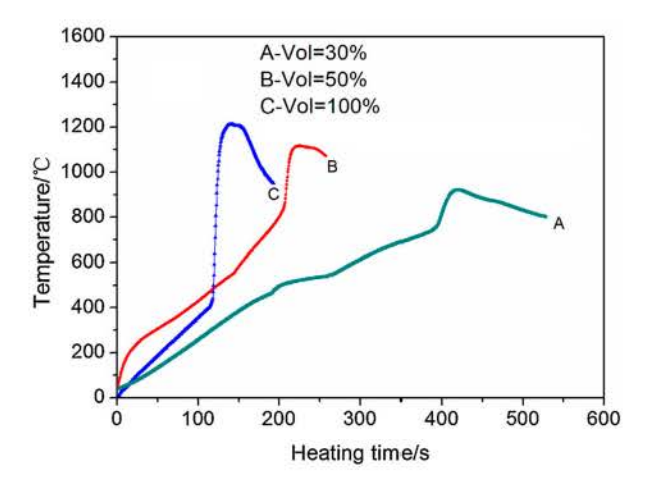


Figure 12. Heating profiles of Al + ZrO₂ powder mixtures in a SiC susceptor-assisted microwave combustion synthesis process, the compositions of the mixtures correspond to the formation of 30 vol.-% (A), 50 vol% (B), and 100 vol.-% (C) of Al₂O₃ + Al₃Zr reinforcing phases. Reprinted from [88], Copyright (2015), with permission from Elsevier.

composite prepared by annealing of the cold-pressed pellets in a vacuum furnace at 1100° C for 10 min (Figure 13). In the microstructure of the composites, the dark background is the Al matrix, rectangular grey particles are the Al₃Zr reinforcement, fine particles prepresent the Al₂O₃ phase.

Aluminium and magnesium matrix composites obtained by induction sintering

As induction sintering is not used as widely as SPS for the production of composites, the available structural

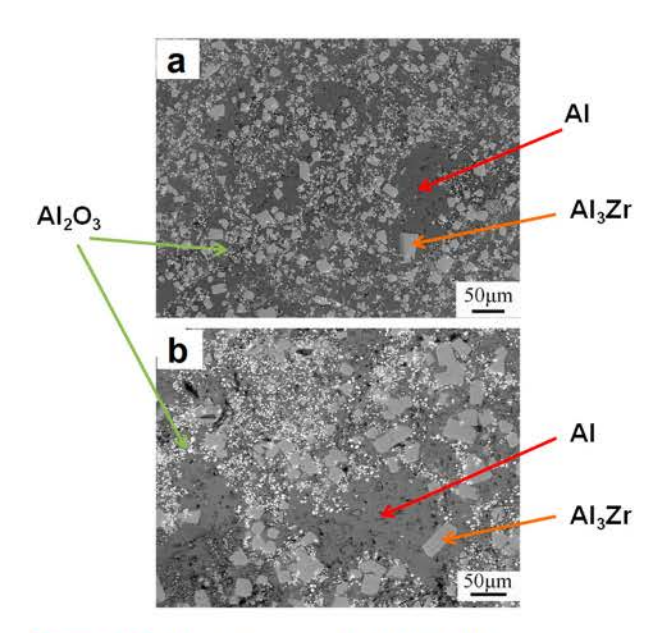


Figure 13. Microstructure of Al-Al₂O₃-Al₃Zr composites obtained by microwave combustion synthesis (a) and synthesis via vacuum furnace annealing (b). Dark back ground – Al matrix, rectangular grey particles – Al₃Zr, fine particles – Al₂O₃. Reprinted from [88], Copyright (2015), with permission from Elsevier.

and mechanical property data are rather limited. Induction heating has been successfully used for producing metallic glass-reinforced composites with Mg and Al alloy matrices [62, 89-91]. Al alloy 520.0 strengthened by Cu₅₄Zr₃₆Ti₁₀ metallic glass particles was obtained in ref. [89]. The composite was sintered by induction heating in a steel die under a pressure of 50 MPa at the maximum temperature of 720 K (which is within the supercooled liquid region of the Cu54-Zr₃₆Ti₁₀ metallic glass) with a holding time at this temperature of 2 min. Although the pressure during sintering was not very high and the holding time was very short, the composite was fully dense. The material featured a uniform distribution of the glassy reinforcement particles in the matrix.

Comparative investigations: the influence of the sintering method on the phase composition and microstructure of the composites

The heating method of the powder mixtures was shown to influence the phase composition of the sintered material. The Al-VC mixtures were sintered by conventional and microwave sintering; the maximum temperature was the same in those experiments (600° C) [92]. In the microwave sintering experiment, the sample was not soaked at the maximum temperature. Under conventional sintering conditions, the mixture was held for 1 h at the maximum temperature. VAl₃ intermetallic formed only in the microwave sintered material and was a result of the interaction between VC and Al. No reaction between the phases was observed in the conventionally sintered material. The authors explained enhanced reactivity of VC towards Al under microwave treatment by high local temperatures developing due to microwave absorption by the vanadium carbide particles. Under conventional sintering, no physical basis was present for increasing the temperature in the vicinity of VC particles. In ref. [93], Al alloy matrix composites containing hybrid reinforcements were developed by microwave and conventional sintering. The microwave process was proved to be more efficient for achieving densification (at the same measured temperature) leading to increased hardness and bending strength despite a 1-h soaking in conventional sintering and the absence of any soaking in the microwave process. Higher densities demonstrated by the microwave sintered samples in comparison with conventionally sintered samples were explained by the volumetric nature of heating in the microwave sintering method. The SiC and TiC particles acted as good absorbers of microwave energy.

Joseph et al. [94] compared the mechanical behaviour of Al matrix composites containing ω-Al-Cu-Fe particles consolidated from a mixture of metallic aluminium and i-Al-Cu-Fe (icosahedral quasicrystalline phase) by hot isostatic pressing and SPS. In composites produced by both methods, copper diffused into the Al matrix leading to the formation of semicoherent precipitates of θ'-Al₂Cu in the case of SPS and incoherent θ-Al₂Cu in the case of hot isostatic pressing. The difference in the structural characteristics of the precipitates was due to a much shorter holding time in the case of SPS. Composites synthesized by the SPS showed a higher proof stress $\sigma_{0.2\%}$ than those obtained by hot isostatic pressing when measured at temperatures below 473 K. An important message of that research is the possibility of the formation of new reinforcing phases of controlled crystalline structure upon the interaction of the matrix metal with the introduced additives.

Mechanical properties of aluminium and magnesium matrix composites obtained by field-assisted sintering

Tables 1-4 summarize the mechanical properties (in compression and tension) of Al-based alloys, Mgbased alloys, Al/Al alloy matrix composites and Mg/ Mg alloy matrix composites obtained by SPS, microwave and induction sintering extracted from the recent literature. Some alloys and composites obtained with the use of field-assisted sintering possess attractive combinations of strength and ductility and can compete with classical cast and wrought materials.

For MMCs obtained by field-assisted sintering, due to the use of high heating rates, grain growth can be controlled such that both the matrix and the reinforcing particles can retain their fine sizes. The following strengthening mechanisms should be considered in MMCs obtained by field-assisted sintering: dispersion strengthening, grain boundary strengthening, dislocation strengthening, solution strengthening and load transfer. Knowing the relative contribution of each mechanism can be useful for the property tailoring of the composites in the required direction.

Grain refinement is a very effective route to improve the strength according to Hall-Petch equation [95]:

$$\sigma_{v} = \sigma_0 + kd^{-1/2},\tag{4}$$

where σ_y is the yield stress of the material with grain size d, σ_0 is the yield stress of the material with coarse grains and k is a chemistry- and microstructure-dependent constant.

The contribution of Orowan strengthening $\Delta \sigma_{Or}$ can be calculated as follows [96]:

$$\Delta \sigma_{Or} = \varphi \frac{Gb}{L} \tag{5}$$

where φ is a constant equal to 2, G is the shear modulus of the matrix, b is the Burgers vector of the matrix and L is the inter-particle distance.

Table 1. Sintering conditions and mechanical properties in compression of aluminium matrix composites and aluminium alloys obtained by field-assisted sintering.

Composition	Sintering conditions	Strain rate, s ⁻¹	Yield strength/ 0.2% proof stress, MPa	Ultimate strength, MPa	Deformation at fracture, %	Reference
Al-Zn-Mg	SPS, 500°C, 10 min, 80 MPa	10 ⁻³	610	736		[97]
Al 2024	SPS, 500°C, 10 min, 50 MPa	3.7 · 10-4	256	-	1 -	[105]
Al 2024+2 wt.% TiN	SPS, 500°C, 10 min, 50 MPa	3.7 · 10-4	730	831	10	[105]
Al+ ω-Al-Cu-Fe + θ'-Al ₂ Cu	SPS, 550°C, 2 min, 100 MPa	1.4 · 10-4	500	-	4	[94]
Al 6082 + ω-Al-Cu-Fe + Al ₂ Cu + i- Al-Cu-Fe + Al ₁₃ Fe ₄	SPS, 550°C, 5 min, 50 MPa	1.8 · 10 ⁻³	519	639	24	[106]
Al (air atomized, ball-milled with stearic acid)	SPS, 600°C, 1 h, 49 MPa	975	440	-	·=	[107]
Al (air atomized)	SPS, 600°C, 1 h, 49 MPa	-	173	_	_	[107]
Al+5 vol% AlCoCrFeNi high- entropy alloy	SPS, 580°C, 10 min, 6 MPa	10 ⁻³	137	7.50	50	[81]
Al 7075 + 15 vol% Zr ₆₅ Cu ₁₈ Ni ₇ Al ₁₀	Cold compaction; SPS, 300° C, 10 min, 600 MPa	5 · 10 ⁻⁴	366	471	25	[77]
Al + 40 vol% Al ₆₅ Cu _{16.5} Ti _{18.5}	SPS, 500°C, 400 MPa	10-3	1100	1710	4.3	[108]
Al + 5 at.% Fe	SPS, 480°C, 5 min, ~100 MPa or greater	10 ⁻³	992	1045	30	[109]
Al 7075+15vol% Ti ₄₈ Zr _{7.5} Cu ₃₉ Fe _{2.5} Sn ₂ Si ₁	Cold compaction; SPS, 300°, 10 min, 600 MPa	5 · 10-4	950	1002	4	[110]
Al+21vol%(TiAl ₃ +Al ₂ O ₃)	Accumulative roll bonding, SPS. 550°C, 102 MPa, 5 min; 700°C, 4 MPa, 5 min	0 0	-	630	20	[111]
Al+25 vol%Ni ₆₀ Nb ₄₀	Microwave sintering, 550° C; hot extrusion, 350°C	8.3 · 10-4	155	375	>50	[112]
Al	Microwave sintering, 550° C; hot extrusion, 350°C	8.3 · 10 ⁻⁴	80	245	>50	[112]
Al 6061 + 30 wt.% Ti(W,C)	Microwave sintering, 560° C, 45 min	3.6· 10 ⁻⁴	236	474	33.5	[87]
Al 6061 + 10 wt.% Ti(W,C)	Microwave sintering, 560° C, 45 min	3.6- 10-4	118	346	39.6	[87]
Al 6061	Microwave sintering, 560° C, 45 min	3.6- 10-4	99	5 7.5 5	197	[87]
Al	Microwave sintering, 550° C; annealing 400°C, 1 h; hot extrusion, 350°C	8.3 · 10 ⁻⁴	(2)	308	9.5	[113]
15 vol% (Al-Li-Cu) + Al	Microwave sintering, 550° C; annealing 400°C, 1 h; hot extrusion, 350°C	8.3 · 10 ⁻⁴	-	453	6.4	[113]
Al 6061 +15 vol% [(Fe _{1/2} Co _{1/2}) ₇₅ B ₂₀ Si ₅] ₉₆ Nb ₄	Induction sintering, 555°C, 2 min, 70 MPa	10 ⁻³	570	600	13	[90]
Al 520.0 + 15 vol% Cu ₅₄ Zr ₃₆ Ti ₁₀	Induction sintering, 447°C, 2 min, 50 MPa	10 ⁻³	580	840	14	[89]
Al 2024 + 15 wt.% $Fe_{73}Nb_{5}Ge_{2}P_{10}C_{6}B_{4} \ metallic$ glass	Induction sintering, 550°C, 30 min, 400 MPa	10 ⁻³	403	660	12	[91]

Solution strengthening can be significant in materials processed by field-assisted sintering, unless conditions of sintering are intentionally selected such that the time and temperature favour decomposition of solid solutions and the formation of precipitates [97], metastable or stable (purposeful aging of alloys during the field-assisted sintering/treatment).

Dislocation strengthening of the matrix is determined by the Taylor formula [95]:

$$\sigma = \sigma_0 + \alpha G b \rho^{1/2}, \tag{6}$$

where σ is the flow stress, G is the shear modulus, b is the Burgers vector, ρ is the dislocation density and α is a material-dependent constant between 0.5 and 1 [96]. In MMCs containing ceramic reinforcements, dislocations can originate from the coefficient of thermal expansion (CTE) mismatch. In addition, in the case of fast consolidation of powders at relatively low temperaures, the matrix metals can retain dislocations

accumulated during the powder processing stage (for example, during mechanical milling).

Similarly to MMCs obtained by conventional methods, composites fabricated by field-assisted sintering can be strengthened by load transfer. As composites produced by sintering are mostly discontinuously reinforced composites, a model elaborated by Nardone and Prewo [98] can be applied. In their work, it was shown that the shear lag theory can be used to describe the strength of discontinuous SiC-reinforced aluminium matrix composites provided that the theory is modified to take into account the tensile transfer of load from the matrix to the discontinuous reinforcement. According to the model, the yield strength of a composite reinforced with whiskers or particles can be calculated as follows:

$$\sigma_{cy} = \sigma_{my} \left[\frac{1}{2} V_r(s+2) + V_m \right]$$
 (7)

where σ_{cy} is the yield strength of the composite, σ_{my} is the yield strength of the unreinforced matrix, s is the

Table 2. Sintering conditions and mechanical properties in tension of aluminium matrix composites and aluminium alloys obtained by field-assisted sintering.

Composition	Sintering conditions	Strain rate, s ⁻¹	Yield strength/ 0.2% proof stress, MPa	Ultimate strength, MPa	Deformation at fracture, %	Reference
Al+1 vol% CNT	SPS, 630°C, 30 min, 30 MPa; hot extrusion, 500°C	5 · 10 ⁻⁴	279	306	12	[75]
AI + A ₄ C ₃ /graphene (from 0.42 wt.%graphene oxide + AI)	SPS, 610°C, 20 min, 50 MPa; hot extrusion	$1.67 \cdot 10^{-3}$	149	178	19	[114]
Al-4Cu + 1 wt.%. reduced graphene oxide	SPS, 500°C, 10 min, 50 MPa;	3.5 · 10 ⁻⁴	139	320	10	[115]
Al+4.5wt.%BN (AlN and AlB ₂ formed in-situ during ball milling and SPS)	SPS, 600°C, 60 min, 50 MPa	~	250	386	5	[116]
Al (ball-milled)	SPS, 600°C, 60 min, 50 MPa	-	160	167		[116]
Al+1wt,%BN nanosheets	SPS, 600°C, 60 min, 50 MPa	_	_	152	6.5	[117]
Al+4wt.%Sc	SPS, 550°C, 2 min, 50 MPa + T6 treatment	=	197	226	11	[118]
Al+0.75vol%CNT	SPS, 630°C, 30 min, 30 MPa; hot rolling, 550°C	2.1 · 10 ⁻³	200	220	21	[119]
Al 2024	SPS, 500°C, 10 min, 50 MPa; thermo-mechanical treatment	5 · 10 ⁻⁴	530	583	16.2	[3]
Al $6061 + 30 \text{ vol}\% \text{ Si}_3\text{N}_4$	SPS, 570 C, 15 min, 50 MPa; heat treatment (solution treatment, aging)	·=.	400	499	1.5	[120]
Al+25 vol%Ni ₆₀ Nb ₄₀	Microwave sintering, 550°C; hot extrusion, 350°C	8.3 · 10 ⁻⁴	102	120	9.5	[112]

aspect ratio of the reinforcement, $s = L_r/d_r$ (L_r is the length and d_r is the diameter of the reinforcement), V_r and V_m is the volume fraction of the reinforcement and the matrix, respectively. This equation predicts a strengthening effect for reinforcement with an aspect ratio s=1.

Interestingly, during SPS of particle-reinforced agglomerates obtained by mechanical milling, microstructures analogous to trimodal composites (as described in ref. [99]) can be obtained. The concept of trimodal architectures is based on combining three components: nano/ultrafine matrix grains, coarse matrix grains and ceramic reinforcements. Such a combination gives opportunities for flexible engineering of the composites' microstructures and mechanical properties. The role of coarse grains is to improve the ductility of otherwise brittle materials. Yang et al. [99] obtained the trimodal composites by adding coarse-grained unreinforced matrix particles to the cryomilled B₄C-Al alloy mixture and subjecting the powder to hot isostatic pressing followed by hot extrusion. A possibility of local temperature differences leading to the formation of bimodal microstructures in metallic materials processed by SPS was considered in refs. [43,100,101]. If a ceramic particle-reinforced powder material is subjected to SPS under such conditions that high-temperature regions develop locally, melting of a fraction of the matrix can take place, leading to a certain redistribution of the phases and the formation of particle-depleted areas of the matrix. Those particle-depleted areas could play a role similar to that played by the coarse matrix grains in trimodal composites.

The bimodal grain structures were found to exhibit deformation and fracture behaviour similar to ductile phase-toughened brittle materials [102]. The ductile coarse grains in the ultrafine-grained matrix impede the propagation of microcracks, which leads to enhanced ductility and toughness. Bimodal-structure alloys can be obtained by field-assisted sintering

Table 3. Sintering conditions and mechanical properties in compression of magnesium matrix composites and magnesium alloys obtained by field-assisted sintering.

Composition	Sintering conditions	Strain rate, s ⁻¹	Yield strength/0.2% proof stress, MPa	Ultimate strength, MPa	Deformation at fracture, %	Reference
AZ91	SPS, 360°C, 1 h	$1.1 \cdot 10^{-3}$	185	341	15.2	[121]
AZ91	SPS, 360°C, 2 h; 200°C, 2 h	$1.1 \cdot 10^{-3}$	217	374	13.9	[121]
Mg + 1Al + 0.15CNT	SPS, 560°C, 5 min; hot extrusion, 400°C	10 ⁻³	118	321	17.9	[122]
Mg-Gd-Zn-Zr (GZ100 K)	SPS, 400°C, 10 min, 50 MPa	10^{-3}	210	386	20	[123]
Mg + 2vol%SiC	SPS, 450°C, 5 min, 50 MPa	10-4		247	9	[124]
AZ80	SPS, 350°C, 3 min, 100 MPa	2.5 · 10-4	442	546	4.2	[101]
Mg AZ31	SPS, 400°C, 5 min, 80 MPa	2.5 · 10-4	400	500	3.6	[125]
Mg	SPS, 400°C, 5 min, 80 MPa	$2.5 \cdot 10^{-4}$	400	500	3.6	[126]
Mg + Mg-Zn alloy	SPS, 400°C, 5 min, 80 MPa	2.5 · 10-4	408	506	6.6	[126]
AZ91 + Zr ₅₇ Nb ₅ Cu _{15.4} Ni _{12.6} Al ₁₀	Induction sintering, 440°C, 2 min, 50 MPa	े र ू	325	542	11	[62]
AZ61 + 3 vol% CNT	Microwave sintering, 500° C, 8 min	-	117	218	10.2	[67]

Table 4. Sintering conditions and mechanica	properties in tension of m	nagnesium matrix composites	and magnesium alloys
obtained by field-assisted sintering.			

Composition	Sintering conditions	Strain rate, s ⁻¹	Yield strength/0.2% proof stress, MPa	Ultimate strength, MPa	Deformation at fracture, %	Reference
Mg	SPS, 585°C, 5 min, 60 MPa	$2.8 \cdot 10^{-3}$	-	120	2	[23]
Mg + 10wt.%SiC	SPS, 585°C, 5 min, 60 MPa	$2.8 \cdot 10^{-3}$	()/-	140	<u></u>	[23]
Mg + 1Al + 0.15CNT	SPS, 560°C, 5 min; hot extrusion, 400°C	10 ⁻³	157	271	8.8	[122]
Mg + 3wt.%Ti ball- milled	SPS, 600°C, 30 min, 30 MPa; hot extrusion, 400°C	5 · 10-4	184	224	14.9	[127]
Mg	Microwave sintering, 640°C, 25 min; hot extrusion, 350°C	1.6 · 10 ⁻⁴	116	168	6.1	[128]
Mg + 2wt.%Y ₂ O ₃	Microwave sintering, 640°C; hot extrusion, 350°C	1.7 · 10 ⁻⁴	157	244	9.1	[129]

methods. In the case of SPS, the bimodal structure can be obtained either by consolidating a mixture of powders with different particle sizes [103] or 'in-situ' by employing the effect of local overheating.

A common problem of materials produced by powder sintering, including field-assisted sintering, is residual porosity, which can vary from fractions of a percent to several percent, unless rendered intentionally high for specific applications. Therefore, the influence of porosity on strength should be taken into account. According to Balshin [104], the tensile strength of a porous metal-ceramic material can be expressed as

$$\sigma_p = \sigma_0 \theta^n, \tag{8}$$

where σ_p is the strength of a material with residual porosity, θ is the relative density, σ_0 is the strength of the zero-porosity material and m is a constant.

Functional properties of selected aluminium and magnesium matrix composites obtained by field-assisted sintering

Thermal and electrical conductivity of aluminium matrix composites

Al-diamond composites are of interest from the viewpoint of developing materials with high thermal conductivity [130,131]. Tan et al. [132] addressed the issue of the nature of the aluminium-diamond interface and distinguished between diffusion-bonded and reaction-bonded interfaces. The diffusion-bonded interface was thought to be preferable for achieving a low thermal resistance. A low thermal conductivity of some composites produced by SPS was explained by the temperature gradients within the sample. Diamond particles located in the high-temperature regions were more likely to develop the reaction-type interfaces (with the formation of Al_4C_3 as the reaction product).

Aluminium matrix composites containing silicon particles are attractive packaging materials for microelectronic applications, as their CTE can be reduced relative to pure aluminium, their thermal conductivity remaining high. By SPS at 510°C, nearly fully dense Si-Al composites were obtained [133]. A composite containing 45 vol.-% Si showed a good combination

of properties: an average CTE of 12.7 10⁻⁶ K⁻¹ and a thermal conductivity of 113 W m⁻¹ K⁻¹. The obtained value of CTE was lower than that of the counterpart materials. The benefit of SPS was in keeping the grains of silicon small during consolidation. A high surface area of silicon particles allowed restraining expansion of the Al phase lowering the CTE of the composite.

It is a serious challenge to fabricate high-strength Al matrix composites without sacrificing their electrical conductivity. It was shown that Al matrix composites can retain a high electrical conductivity (at the level of unreinforced aluminium) and become stronger than pure aluminium when few-layer graphene joined to the Al matrix by Al₄C₃ nanorods acts as a reinforcement [114]. The electrical conductivity of the composite having a yield strength of 149 MPa and an ultimate tensile strength of 178 MPa was 59.8% of the International Annealed Copper Standard (%IACS). The synthesized material was, therefore, recommended as a high-performance conductor.

Biocompatibility and biodegradability of magnesium matrix composites

Magnesium-based composites are suitable for biomedical applications. As microstructural refinement is beneficial for magnesium alloys designed for temporary implants, SPS is considered as a processing method for these alloys. Currently, SPS of magnesium matrix composites and Mg-based alloys is studied with the prospects of developing biodegradable materials [134–140].

Microwave sintering was used for making porous Mg-based composites as candidate biodegradable materials [141]. A Si₃N₄ powder or an Al₂O₃ whisker additive was introduced into the Mg matrix to modify its electrochemical performance. As Si₃N₄ absorbs microwaves, higher local temperatures caused explosive evaporation and formation of larger pores compared with composites containing Al₂O₃.

Scale-up of the field-assisted sintering processes

The key problem of the scale-up of the sintering processes is to ensure the same temperature in the laboratory-size and industrial-size sintered parts. The temperature distribution in specimens differing in electrical conductivity has been addressed in ref. [142] for the SPS process in a die. It was shown that, for conductive materials, the temperature in the centre of a disk-shaped specimen is higher than in the rim areas. The predictive capability of modelling approaches is of great importance for the industrial implementation of SPS. The scalability of SPS was analysed experimentally and theoretically by Olevsky et al. [143,144]. In those studies, scalability experiments on the SPS of similarly shaped alumina specimens of the four different sizes have been conducted. The processed specimens have been characterized in terms of relative density and grain-pore structure. Overall, SPS showed good scalability potential. At the same time, it was shown that, due to the demonstrated possibility of a significant size impact in case of high heating rates and large specimen sizes, the predictive capability of reliable modelling approaches is of great importance for the industrial implementation of the SPS technique.

In the area of metallic materials, Tokita [145] reported the commercial use of metallic sputtering targets 99-100% dense, 5-20 mm thick and 300-350 mm in diameter obtained by SPS. An advanced SPS approach enabling the scale-up fabrication of large size complex shapes and an energy-efficient processing has been described in ref. [146]. A unique configuration using deformable and electrically insulated interfaces has been employed to constrain the electric current path for a significant reduction of the electric current required to heat the 40 mm specimen while imposing a gear shape onto the processed parts. A comprehensive electrothermal-mechanical simulation of the SPS process revealed that the high thermal stability observed for this SPS approach originates from different factors: the high thermal conductivity of the metal powder and the thermal confinement of this metal powder via the lateral thermal contact resistance and via the upper and lower alumina powder which has a very low thermal conductivity. That case study demonstrated the high scalability potential of the SPS technology which can combine the benefits of advanced material properties (through high pressures, high heating rates) and complex shapes. It is theoretically possible to place any number of complex shape interfaces in a large-dimension tooling set (like in a conventional furnace), improving drastically the productivity and, in turn, the scalability of the SPS technology. Such an improvement would require perfect control of the temperatures and a homogeneous displacement field of the powder.

Comparative studies of SPS and hot pressing were reported by Musa et al. [147] for Ti-38 vol.-% Al₂O₃-11.5 vol.-%TiC composites: only 5 min was needed to sinter the material by SPS and about 5 h was needed to do the same using HP. In both cases, relative densities greater than 99.9% were reached. The times given are a sum of the duration of the heating stage and the dwell time at the maximum temperature. The total energies required for the SPS and hot pressing runs were compared to reveal that the SPS technology allowed for energy saving of 90-95%. Notably, the use of graphite felt around the die to reduce heat losses by radiation was found to lead to energy savings of 25% under the selected sintering conditions.

As Kelly & Graeve pointed out [148], highthroughput SPS systems will have a serious impact on mass production. It was emphasized that lessons learnt during the development of the hot pressing technology can be directly applied to SPS to minimize the associated risks. An ideal SPS design for manufacturing would be a fully automated process, from loading and handling of the die to sintering, cooling and sample removal from the die. The key difference between hot pressing and SPS is the method of heating. When SPS is used instead of hot pressing, the processing times are significantly reduced; some processes require lower temperatures. The reduced times and temperatures in the SPS processes lead to reduced energy consumption (and energy cost) per sample. Since, within a given time, SPS will produce a larger number of parts than hot pressing, the sintering cost (which includes the operation of the cooling system, cosumables and burden costs and is taken to be the same for SPS and hot pressing in ref. [148]) per sample will be lower for the SPS technology than for hot pressing. A higher productivity and a better expandability of SPS relative to hot pressing have also been highlighted in ref. [149].

The scalability of microwave sintering is often difficult to achieve [36]. The results obtained by Manière et al. [150,151] provide a basis for explaining the inherent instability and non-reproducibility of the experiments frequently reported in the literature for microwave sintering. The process instabilities stem from the intrinsic non-homogeneous electromagnetic fields repartition and their sensitivity to the presence of dissipative materials, such as aluminium and magnesium matrix composites, during microwave sintering [39,113,128]. The direct microwave heating configuration, for large-scale specimens, results in the formation of a hot spot at the centre of the sample. The hot spot phenomenon increases drastically in the beginning of the process and then stabilizes when the densification occurs resulting, at the end of the heating cycle, in a significant temperature difference across the sample's volume. The microwave field penetration and then the heating become more superficial when the densification happens; this fact explains the temperature gradients' stabilization. The sample shape is highly



deformed during the densification due to the hot spot formation but tends to go back to the cylindrical shape at the end of the densification. A decrease in the sample size appears to reduce the thermal gradients and, at the same time, it resolves the problem of densification heterogeneities. Sintering of small samples is, therefore, more stable. The temperature inhomogeneity can be balanced by the use of susceptors ('hybrid microwave heating'), which can add an external heat flux uniformizing the temperature inside the sample [150,151]. The hybrid heating configuration succeeds in reducing the temperature gradients in the sample, allowing a more uniform and scalable overall densification of the large samples.

Induction sintering provides fast heating and cooling, dramatically shortens the sintering time and ensures high energy efficiency. The scalability of the induction sintering process can be achieved if the cross-sections of the coil and the sintered part are similar with small gaps between them and if undesirable thermal gradients are avoided by selecting optimal heating rates and penetration depths [18].

Summary

The overview of the literature on the processing, microstructure and properties of Al- and Mg-based materials produced by field-assisted sintering shows that composites and alloys with high strength and high ductility can be obtained by powder metallurgy through the flexible compositional and microstructural design and a proper choice of the field-assisted sintering parameters. Traditional MMC compositions (MMCs reinforced with ceramic particles) as well as composites reinforced with particles of alloys (metallic glass, high-entropy alloys, derivatives of quasicrystals) are currently of interest. MMCs with metallic glass reinforcements present a rapidly developing research direction. The very possibility of consolidating the metal matrix-metallic glass mixtures while preserving the amorphous state of the reinforcement depends on the sintering method. SPS and microwave sintering have been successfully used for the production of functional Al- and Mg-based materials (materials with high thermal and electrical conductivity, biodegradable materials). Processes of local character (overheating, melting, infiltration, chemical reactions) play significant roles in the microstructure formation and property variation of the composites obtained by SPS and microwave sintering. The scale of locality is determined by either the initial particle size or the distance between inclusions in a matrix. The progress in the microstructural and compositional design of the composites made over recent years is a solid basis for the development of commercial products.

Disclosure statement

No potential conflict of interest was reported by the author(s).

Funding

This work was partially funded by the Ministry of Science and Higher Education of the Russian Federation, project 075-15-2020-781. The support of the National Science Foundation, USA, Grant DMR-1900876 is gratefully acknowledged.

References

- [1] Hirsch J. Recent development in aluminium for automotive applications. Trans Nonferrous Met Soc China. 2014;24:1995-2002.
- [2] German RM. Sintering: from empirical observations to scientific principles. Oxford: Butterworth-Heinemann; 2014.
- [3] Zheng R, Sun Y, Ameyama K, et al. Optimizing the strength and ductility of spark plasma sintered Al2024 alloy by conventional thermo-mechanical treatment. Mater Sci Eng A. 2014;590:147-152.
- [4] Song J, She J, Chen D, et al. Latest research advances on magnesium and magnesium alloys worldwide. J Magnesium Alloys. 2020;8:1-41.
- [5] Torralba JM, da Costa CE, Velasco F. P/M aluminum matrix composites: an overview. J Mater Proc Tech. 2003;133:203-206.
- [6] Saheb N, Iqbal Z, Khalil A, et al. Spark plasma sintering of metals and metal matrix nanocomposites: a review. J Nanomater. 2012;2012:983470.
- [7] Sharma N, Alam SN, Ray BC. Fundamentals of spark plasma sintering (SPS): an ideal processing technique for fabrication of metal matrix nanocomposites. In: P Cavaliere, editor. Spark plasma sintering of materials: advances in processing and applications. Cham: Springer Nature Switzerland AG; 2019. p. 21-59.
- [8] Matli PR, Shakoor RA, Mohamed Amer Mohamed A, et al. Microwave rapid sintering of Al-metal matrix composites: a review on the effect of reinforcements, microstructure and mechanical properties. Metals. 2016;6:143.
- [9] Awotunde MA, Adegbenjo AO, Obadele BA, et al. Influence of sintering methods on the mechanical properties of aluminium nanocomposites reinforced with carbonaceous compounds: a review. J Mater Res Technol. 2019;8:2432-2449.
- [10] Weston NS, Thomas B, Jackson M. Processing metal powders via field assisted sintering technology (FAST): a critical review. Mater Sci Technol. 2019;35:1306-1328.
- [11] Tokita M. Trends in advanced SPS spark plasma sintering systems and technology. Functionally gradient materials and unique synthetic processing methods from next generation of powder technology.. J Soc Powder Technol Japan. 1993;30:790-804.
- [12] Tokita M. Development of advanced spark plasma sintering (SPS) systems and its industrial applications. Ceram Trans. 2006;194:51-59.
- [13] Tokita M. Spark plasma sintering (SPS) method, systems and applications. In: S Somiya, editor. Handbook of advanced ceramics: materials, applications, processing and properties. 2nd ed.

- - Waltham; Oxford; Amsterdam: Academic Press; 2013. p. 1149-1177.
- [14] Munir ZA, Anselmi-Tamburini U, Ohyanagi M. The effect of electric field and pressure on the synthesis and consolidation of materials: a review of the spark plasma sintering method. J Mater Sci. 2006;41:763-777.
- [15] Munir ZA, Quach D, Ohyanagi M. Electric current activation of sintering: a review of the pulsed electric current sintering process. J Am Ceram Soc. 2011;94:1-19.
- [16] Mamedov V. Spark plasma sintering as advanced PM sintering method. Powder Metall. 2002;45:322-
- [17] Olevsky EA, Aleksandrova EV, Ilyina AM, et al. Outside mainstream electronic databases: review of studies conducted in the USSR and post-soviet countries on electric current-assisted consolidation of powder materials. Materials. 2013;6:4375-4440.
- [18] Olevsky EA, Dudina DV. Field-assisted sintering: science and applications. Cham: Springer International Publishing; 2018, 425 p.
- [19] Dudina DV, Bokhonov BB, Olevsky EA. Fabrication of porous materials by spark plasma sintering: a review. Materials. 2019;12:541.
- [20] Olevsky E, Froyen L. Constitutive modeling of sparkplasma sintering of conductive materials. Scr Mater. 2006;55:1175-1178.
- [21] Lee G, Manière C, McKittrick J, et al. Electric current effects in spark plasma sintering: from the evidence of physical phenomenon to constitutive equation formulation. Scr Mater. 2019;170:90-94.
- [22] Huntington HB. Electromigration in metals. In: Nowick AS, Burton JJ, editors. Diffusion in solids: recent developments. New York; London: Academic Press; 1975. p. 303-352.
- [23] Nur Azrina Wan Muhammad W, Sajuri Z, Mutoh Y, et al. Microstructure and mechanical properties of magnesium composites prepared by spark plasma technology. J Alloys 2011;509:6021-6029.
- [24] Xü CY, Jia SS, Cao ZY. Synthesis of Al-Mn-Ce alloy by the spark plasma sintering. Mater Charact. 2005;54:394-398.
- [25] Hulbert DM, Anders A, Dudina DV, et al. The absence of plasma in "spark plasma sintering". J Appl Phys. 2008;104:033305.
- [26] Saunders T, Grasso S, Reece MJ. Plasma formation during electric discharge (50 V) through conductive powder compacts. J Eur Ceram Soc. 2015;35:871-877.
- [27] Song X, Liu X, Zhang J. Neck formation and selfadjusting mechanism of neck growth of conducting powders in spark plasma sintering. J Am Ceram Soc. 2006;89:494-500.
- [28] Kuz'mov AV, Olevskii EA, Aleksandrova EV. Effect of micrononuniform heating of powder in fieldassisted sintering on shrinkage kinetics. Powder Metall Metal Ceram. 2013;51:657-665.
- [29] Collard C, Trzaska Z, Durand L, et al. Theoretical and experimental investigations of local overheating at particle contacts in spark plasma sintering. Powder Technol. 2017;321:458-470.
- [30] Dudina DV, Bokhonov BB. Elimination of oxide films during spark plasma sintering of metallic powders: a case study using partially oxidized nickel. Adv Powder Technol. 2017;28:641-647.

- [31] Li XP, Yan M, Imai H, et al. The critical role of heating rate in enabling the removal of surface oxide films during spark plasma sintering of Al-based bulk metallic glass powder. J Non-Cryst Solids. 2013;375:95-
- [32] Xu P, Feng Y, Xu B, et al. Disruption of oxide films during spark plasma sintering of micrometric-sized Al powders and its effect on microstructure and tensile properties of the consolidated Al. J Alloys Compd. 2017;712:822-832.
- [33] Kitchen HJ, Vallance SR, Kennedy JL, et al. Modern microwave methods in solid-state inorganic materials chemistry: from fundamentals to manufacturing. Chem Rev. 2014;114:1170-1206.
- [34] Rosa R, Veronesi P, Leonelli C. A review on combustion synthesis intensification by means of microwave energy. Chem Eng Proc. 2013;71:2-18.
- [35] Gedevanishvili S, Agrawal D, Roy R. Microwave combustion synthesis and sintering of intermetallics and alloys. J Mater Sci Lett. 1999;18:665-668.
- [36] Rybakov KI, Olevsky EA, Krikun EV. Microwave sintering: fundamentals and modeling. J Amer Ceram Soc. 2013;96:1003-1020.
- [37] Agrawal D. Microwave sintering of ceramics, composites and metallic materials, and melting of glasses. Trans Indian Ceram Soc. 2006;65:129-144.
- [38] Wong WLE, Gupta M. Characteristics of aluminum and magnesium based nanocomposites processed using hybrid microwave sintering. J Microwave Power Electromagn Energy. 2010;44:14-27.
- [39] Wong WLE, Gupta M. Using microwave energy to synthesize light weight/energy saving magnesium based materials: a review. Technologies. 2015;3:1-18.
- [40] Hermel W, Leitner G, Krumphold R. Review of induction sintering: fundamentals and applications. Powder Metall. 1980;23:130-135.
- [41] Guyon A, Bouvard D, Chaix JM, et al. Densification and microstructure changes of micron size nickel powder during direct induction sintering. Powder Metall. 2014;57:54-60.
- [42] Xie G, Ohashi O, Yoshioka T, et al. Effect of interface behavior between particles on properties of pure Al powder compacts by spark plasma sintering. Mater Trans. 2001;42:1846-1849.
- [43] Kubota M, Wynne BP. Electron backscattering diffraction analysis of mechanically milled and spark plasma sintered pure aluminium. Scr Mater. 2007;57:719-722.
- [44] Cheng Y, Cui Z, Cheng L, et al. Effect of particle size on densification of pure magnesium during spark plasma sintering. Powder Adv Technol. 2017;28:1129-1135.
- [45] Mendoza-Duarte JM, Robles-Hernandez FC, Estrada-Guel I, et al. Aluminum sintering in air atmosphere using high frequency induction heating. Microscopy Microanal. 2017;23(S1):1950-1951.
- [46] Mortensen A, Llorca J. Metal matrix composites. Annu Rev Mater Res. 2010;40:243-270.
- [47] Llorca J, Needleman A, Suresh S. An analysis of the effects of matrix void growth on deformation and ductility in metal-ceramic composites. Acta Metall Mater. 1991;39:2317-2335.
- [48] Ghasali E, Shirvanimoghaddam K, Pakseresht AH, et al. Evaluation of microstructure and mechanical properties of Al-TaC composites prepared by spark plasma sintering process. J Alloys Compd. 2017;705:283-289.



- [49] Pakdel A, Witecka A, Rydzek G, et al. A comprehensive microstructural analysis of Al-WC micro- and nano-composites prepared by spark plasma sintering. Mater Des. 2017;119:225-234.
- [50] Aliyu IK, Saheb N, Hassan SF, et al. Microstructure and properties of spark plasma sintered aluminum containing 1 wt.% SiC nanoparticles. Metals. 2015;5:70-83.
- [51] Penchal Reddy M, Shakoor RA, Parande G, et al. Enhanced performance of nano-sized SiC reinforced Al metal matrix nanocomposites synthesized through microwave sintering and hot extrusion techniques. Prog Nat Sci Mater Int. 2017;27:606-614.
- [52] Dash K, Chaira D, Ray BC. Synthesis and characterization of aluminium-alumina micro- and nanocomposites by spark plasma sintering. Mater Res Bull. 2013;48:2535-2542.
- [53] Leszczyńska-Madej B, Garbiec D, Madej M. Effect of sintering temperature on microstructure and selected properties of spark plasma sintered Al-SiC composites. Vacuum. 2019;164:250-255.
- [54] Sweet GA, Brochu M, Hexemer Jr RL, et al. Consolidation of aluminum-based metal matrix composites via spark plasma sintering. Mater Sci Eng A. 2015;648:123-133.
- [55] Bolzon G, Chiarullo EJ, Egizabal P, et al. Constitutive modelling and mechanical characterization of aluminium-based metal matrix composites produced by spark plasma sintering. Mech Mater. 2010;42:548-558.
- [56] Ghasali E, Alizadeh M, Ebadzadeh T, et al. Investigation on microstructural and mechanical properties of B₄C-aluminum matrix composites prepared by microwave sintering. J Mater Res Technol. 2015;4:411-415.
- [57] Bhatt J, Balachander N, Shekher S, et al. Synthesis of nanostructured Al-Mg-SiO₂ metal matrix composites using high-energy ball milling and spark plasma sintering. J Alloys Compd. 2012;536:S35-S40.
- [58] Yaghobizade O, Nazari M, Mashhadi M. The effect of rapid microwave sintering process on the electrical conductivity, thermal conductivity and mechanical properties of Al-TiC composites. Mater Res. 2018;21:e20180324.
- [59] Zhang H, Feng P, Akhtar F. Aluminium matrix tungsten aluminide and tungsten reinforced composites by solid-state diffusion mechanism. Sci Rep. 2017;7:12391.
- [60] Park K, Park J, Kwon H. Fabrication and characterization of Al-SUS316L composite materials manufactured by the spark plasma sintering process. Mater Sci Eng A. 2017;691:8-15.
- [61] Inoue A. Stabilization of metallic supercooled liquid and bulk amorphous alloys. Acta Mater. 2000;48:279-306.
- [62] Dudina DV, Georgarakis K, Li Y, et al. A magnesium alloy matrix composite reinforced with metallic glass. Comp Sci Technol. 2009;69:2734-2736.
- [63] George EP, Raabe D, Ritchie RO. High-entropy alloys. Nature Rev. 2019;4:515-534.
- [64] Huttunen-Saarivirta E. Microstructure, fabrication and properties of quasicrystalline Al-Cu-Fe alloys: a review. J Alloys Compd. 2004;363:154-178.
- [65] Kurita H, Kwon H, Estili M, et al. Multi-walled carbon nanotube-aluminium matrix composites prepared by combination of hetero-agglomeration method, spark plasma sintering and hot extrusion. Mater Trans. 2011;52(10):1960-1965.

- [66] Singh LK, Bhadauria A, Oraon A, et al. Spark plasma sintered Al-0.5 wt% MWCNT nanocomposite: effect of sintering pressure on the densification behavior and multi-scale mechanical properties. Diamond Relat Mater. 2019;91:144-155.
- [67] Akinwekomi AD, Law WC, Tang CY, et al. Rapid microwave sintering of carbon nanotube-filled AZ61 magnesium alloy composites. Composites B Eng. 2016;93:302-309.
- [68] Bhadauria A, Singh LK, Laha T. Combined strengthening effect of nanocrystalline matrix and graphene nanoplatelet reinforcement on the mechanical properties of spark plasma sintered aluminum based nanocomposites. Mater Sci Eng A. 2019;749:14-26.
- [69] Kwon H, Leparoux M, Kawasaki A. Functionally graded dual-nanoparticulate-reinforced aluminium matrix bulk materials fabricated by spark plasma sintering. J Mater Sci Technol. 2014;30:736-742.
- [70] Liu XQ, Li CJ, You X, et al. Size-dependent effects of Ti powders in the pure aluminum matrix composites reinforced by carbon nanotubes. J Alloys Compd. 2020;823:153824.
- [71] Kim WJ, Yu YJ. The effect of the addition of multiwalled carbon nanotubes on the uniform distribution of TiC nanoparticles in aluminum nanocomposites. Scr Mater. 2014;72-73:25-28.
- [72] Dudina DV, Mukherjee AK. Reactive spark plasma sintering: successes and challenges of nanomaterial synthesis. J Nanomater. 2013;2013:1-12.
- [73] Rodríguez C, Belzunce FJ, Betegón C, et al. Nanostructured Al-ZrAl₃ materials consolidated via spark plasma sintering: evaluation of their mechanical properties. J Alloys Compd. 2013;550:402–405.
- [74] Duan DZ, Xiao B, Liu JS, et al. Microstructure and performance of diamond composites fabricated by self-propagating high-temperature synthesis using high-frequency induction as a heat source. Int J Refract Metals Hard Mater. 2018;70:39-44.
- [75] Guo B, Song M, Yi J, et al. Improving the mechanical properties of carbon nanotubes reinforced pure aluminum matrix composites by achieving non-equilibrium interface. Mater Des. 2017;120:56-65.
- [76] Zhou W, Bang S, Kurita H, et al. Interface and interfacial reactions in multi-walled carbon nanotubereinforced aluminum matrix composites. Carbon. 2016;96:919-928.
- [77] Wang Z, Georgarakis K, Nakayama K, et al. Microstructure and mechanical behavior of metallic glass fiber-reinforced Al alloy matrix composites. Sci Rep. 2016;6:24384.
- [78] Firestein KL, Steinman AE, Golovin IS, et al. Fabrication, characterization, and mechanical properties of spark plasma sintered Al-BN nanoparticle composites. Mater Sci Eng A. 2015;642:104-112.
- Guan HD, Li CJ, Gao P, et al. Aluminum matrix composites reinforced with metallic glass particles with core-shell structure. Mater Sci Eng A. 2020;771:138630.
- [80] Yuan Z, Tian W, Li F, et al. Microstructure and properties of high-entropy alloy reinforced aluminum matrix composites by spark plasma sintering. J Alloys Compd. 2019;806:901-908.
- [81] Liu Y, Chen J, Li Z, et al. Formation of transition layer and its effect on mechanical properties of AlCoCrFeNi high-entropy alloy/Al composites. J Alloys Compd. 2019;780:558-564.

- [82] Tan Z, Wang L, Xue Y, et al. High-entropy alloy particle reinforced Al-based amorphous alloy composite with ultrahigh strength prepared by spark plasma sintering. Mater Des. 2016;109:219-226.
- [83] Dudina DV, Bokhonov BB, Batraev IS, et al. Interaction between Fe₆₆Cr₁₀Nb₅B₁₉ metallic glass and aluminum during spark plasma sintering. Mater Sci Eng A. 2021;799:140165.
- [84] Lalet G, Kurita H, Miyazaki T, et al. Microstructure of a carbon fiber-reinforced aluminum matrix composite fabricated by spark plasma sintering in various pulse conditions. J Mater Sci. 2014;49:3268-3275.
- [85] Thakur SK, Kong TS, Gupta M. Microwave synthesis and characterization of metastable (Al/Ti) and hybrid (Al/Ti + SiC) composites. Mater Sci Eng A. 2007;452-453:61-69.
- [86] Ghasali E, Pakseresht AH, Agheli M, et al. WC-Co particles reinforced aluminum matrix by conventional and microwave sintering. Mater Res. 2015;18:1197-1202.
- [87] Zheng RR, Wu Y, Liao SL, et al. Microstructure and mechanical properties of Al/(Ti,W)C composites prepared by microwave sintering. J Alloys Compd. 2014;590:168-175.
- [88] Zhu H, Hua B, Cui T, et al. Microwave combustion synthesis of in situ Al2O3 and Al3Zr reinforced aluminum matrix composites. Mater Res Bull. 2015;68:283-288.
- [89] Dudina DV, Georgarakis K, Li Y, et al. Cu-based metallic glass particle additions to significantly improve overall compressive properties of an Al alloy. Composites A Appl Sci Manuf. 2010;41:1551-1557.
- [90] Aljerf M, Georgarakis K, Louzguine-Luzgin D, et al. Strong and light metal matrix composites with metallic glass particulate reinforcement. Mater Sci Eng A. 2012;532:325-330.
- [91] Zheng R, Yang H, Liu T, et al. Microstructure and mechanical properties of aluminum alloy matrix composites reinforced with Fe-based metallic glass particles. Mater Des. 2014;53:512-518.
- [92] Ghasali E, Orooji Y, Germi HN. Investigation on insitu formed Al₃V-Al-VC nano composite through conventional, microwave and spark plasma sintering. Heliyon. 2019;5:e01754.
- [93] Ghasali E, Yazdani-rad R, Asadian K, et al. Production of Al-SiC-TiC hybrid composites using pure and 1056 aluminum powders prepared through microwave and conventional heating methods. J Alloys Compd. 2017;690:512-518.
- [94] Joseph A, Gauthier-Brunet V, Joulain A, et al. Mechanical properties of Al/ω-Al-Cu-Fe composites synthesized by the SPS technique. Mater Charact. 2018;145:644-652.
- [95] Cordero ZC, Knight BE, Schuh CA. Six decades of the Hall-Petch effect - a survey of grain-size strengthening studies on pure metals. Int Mater Rev. 2016;61(8):495-512.
- [96] Miller WS, Humphreys FJ. Strengthening mechanisms in particulate metal matrix composites. Scr. Metall. Mater. 1991;25:33-38.
- [97] Queudet H, Lemonnier S, Barraud E, et al. One-step consolidation and precipitation hardening of an ultrafine-grained Al-Zn-Mg alloy powder by spark plasma sintering. Mater Sci Eng A. 2017;685:227-234.
- [98] Nardone VC, Prewo KM. On the strength of discontinuous silicon carbide reinforced aluminum composites. Scr Metall. 1986;20:43-48.

- [99] Yang H, Topping TD, Wehage K, et al. Tensile behavior and strengthening mechanisms in a submicron B₄C-reinforced Al trimodal composite. Mater Sci Eng A. 2014;616:35-43.
- [100] Pozuelo M, Melnyk C, Kao WH, et al. Cryomilling and spark plasma sintering of nanocrystalline magnesium-based alloy. J Mater Res. 2011;26:904-911.
- [101] Zheng B, Ertorer O, Li Y, et al. High strength, nanostructured Mg-Al-Zn alloy. Mater Sci Eng A. 2011;528:2180-2191.
- [102] Lee Z, Radmilovic V, Ahn B, et al. Tensile deformation and fracture mechanism of bulk bimodal ultrafine-grained Al-Mg alloy. Metall Mater Trans A. 2010;41:795-801.
- [103] Tian W, Li S, Chen X, et al. Intergranular corrosion of spark plasma sintering assembled bimodal grain sized AA7075 aluminum alloys. Corrosion Sci. 2016;107:211-224.
- [104] Balshin MY. The dependence of mechanical properties of powder metals on porosity and the ultimate properties of porous metal-ceramic materials. Dokl Askd SSSR. 1949;67:831-834. (in Russian).
- [105] Li B, Sun F, Cai Q, et al. Effect of TiN nanoparticles on microstructure and properties of Al2024-TiN nanocomposite by high energy milling and spark plasma sintering. J Alloys Compd. 2017;726:638-650.
- [106] Shadangi Y, Sharma S, Shivam V, et al. Fabrication of Al-Cu-Fe quasicrystal reinforced 6082 aluminium matrix nanocomposites through mechanical milling and spark plasma sintering. J Alloys Compd. 2020;828:154258.
- [107] Kubota M. Properties of nano-structured pure Al produced by mechanical grinding and spark plasma sintering. J Alloys Compd. 2007;434-435:294-297.
- [108] Tan Z, Wang L, Xue Y, et al. A multiple grain size distributed Al-based composite consist of amorphous/nanocrystalline, submicron grain and micron grain fabricated through spark plasma sintering. J Alloys Compd. 2018;737:308-316.
- [109] Sasaki TT, Mukai T, Hono K. A high-strength bulk nanocrystalline Al-Fe alloy processed by mechanical alloying and spark plasma sintering. Scr Mater. 2007;57:189-192.
- [110] Wang Z, Xie MS, Zhang WW, et al. Achieving superhigh strength in an aluminum based composite by reinforcing metallic glassy flakes. Mater Lett. 2020;262:127059.
- [111] Zhang GP, Mei QS, Chen F, et al. Production of a high strength Al/(TiAl₃ + Al₂O₃) composite from an Al-TiO₂ system by accumulative roll-bonding and spark plasma sintering. Mater Sci Eng A. 2019;752:192-198.
- [112] Jayalakshmi S, Gupta S, Sankaranarayanan S, et al. Structural and mechanical properties of Ni₆₀Nb₄₀ amorphous alloy particle reinforced Al-based composites produced by microwave-assisted rapid sintering. Mater Sci Eng A. 2013;581:119-127.
- Penchal Reddy M, Manakari V, Parande G, et al. Structural, mechanical and thermal characteristics of Al-Cu-Li particle reinforced Al-matrix composites synthesized by microwave sintering and hot extrusion. Composites B Eng. 2019;164:485-492.
- [114] Zhou W, Mikulova P, Fan Y, et al. Interfacial reaction induced efficient load transfer in few-layer graphene reinforced Al matrix composites for highperformance conductor. Composites B Eng. 2019;167:93-99.



- [115] Khoshghadam-Pireyousefan M, Rahmanifard R, Orovcik L, et al. Application of a novel method for fabrication of graphene reinforced aluminum matrix nanocomposites: synthesis, microstructure, and mechanical properties. Mater Sci Eng A. 2020;772:138820.
- [116] Firestein KL, Corthay S, Steinman AE, et al. Highstrength aluminum-based composites reinforced with BN, AlB2 and AlN particles fabricated via reactive spark plasma sintering of Al-BN powder mixtures. Mater Sci Eng A. 2017;681:1-9.
- [117] Yusupov KU, Corthay S, Bondarev AV, et al. Spark plasma sintered Al-based composites reinforced with BN nanosheets exfoliated under ball milling in ethylene glycol. Mater Sci Eng A. 2019;745:74-81. doi:10.1016/j.msea.2018.12.040
- [118] Cooke RW, Kraus NP, Bishop DP. Spark plasma sintering of aluminum powders prealloyed with scandium additions. Mater Sci Eng A. 2016;657:71-
- [119] Guo B, Ni S, Yi J, et al. Microstructures and mechanical properties of carbon nanotubes reinforced pure aluminum composites synthesized by spark plasma sintering and hot rolling. Mater Sci Eng A. 2017;698:282-288.
- [120] Jiang H, Xu Z, Xiu Z, et al. Effects of pulse conditions on microstructure and mechanical properties of Si₃N₄/6061Al composites prepared by spark plasma sintering (SPS). J Alloys Compd. 2018;763:822-834.
- [121] Mondet M, Barraud E, Lemonnier S, et al. Optimisation of the mechanical properties of a spark plasma sintered (SPS) magnesium alloy through a post-sintering in-situ precipitation treatment. J Alloys Compd. 2017;698:259-266.
- [122] Yan Y, Zhang H, Fan J, et al. Improved mechanical properties of Mg matrix composites reinforced with Al and carbon nanotubes fabricated by spark plasma sintering followed by hot extrusion. J Mater Res. 2016;31:3745-3756.
- [123] Luo Y, Wu Y, Deng Q, et al. Microstructures and mechanical properties of Mg-Gd-Zn-Zr alloys prepared by spark plasma sintering. J Alloys Compd. 2020;820:153405.
- [124] Das A, Harimkar SP. Effect of graphene nanoplate and silicon carbide nanoparticle reinforcement on mechanical and tribological properties of spark plasma sintered magnesium matrix composites. J Mater Sci Technol. 2014;30:1059-1070.
- [125] Guan D, Mark Rainforth W, Sharp J, et al. On the use of cryomilling and spark plasma sintering to achieve high strength in a magnesium alloy. J Alloys Compd. 2016;688:1141-1150.
- [126] Guan D, Gao J, Sharp J, et al. Enhancing ductility and strength of nanostructured Mg alloy by in-situ powder casting during spark plasma sintering. J Alloys Compd. 2018;769:71-77.
- [127] Umeda J, Kawakami M, Kondoh K, et al. Microstructural and mechanical properties of titanium particulate reinforced magnesium composite materials. Mater Chem Phys. 2010;123:649-657.
- [128] Wong WLE, Gupta M. Development of Mg/Cu nanocomposites using microwave assisted rapid sintering. Comp Sci Technol. 2007;67:1541-1552.
- [129] Tun KS, Gupta M. Effect of heating rate during hybrid microwave sintering on the tensile properties of magnesium and Mg/Y2O3 nanocomposite. J Alloys Compd. 2008;466:140-145.

- [130] Chu K, Jia C, Liang X, et al. Effect of sintering temperature on the microstructure and thermal conductivity of Al/diamond composites prepared by spark plasma sintering. Int J Miner Metall Mater. 2010;17:234-240.
- [131] Chu K, Jia C, Liang X, et al. Effect of particle size on the microstructure and thermal conductivity of Al/ diamond composites prepared by spark plasma sintering. Rare Met. 2009;28:646-650.
- [132] Tan Z, Ji G, Addad A, et al. Tailoring interfacial bonding states of highly thermal performance diamond/Al composites: spark plasma sintering vs. vacuum hot pressing. Composites A Appl Sci Manuf. 2016;91:9-19.
- [133] Yu JH, Wang CB, Shen Q, et al. Preparation and properties of Si_p/Al composites by spark plasma sintering. Mater Des. 2012;41:198-202. doi:10.1016/j. matdes.2012.05.007
- [134] Minárik P, Zemková M, Lukác F, et al. Microstructure of the novel biomedical Mg-4Y-3Nd alloy prepared by spark plasma sintering. J Alloys Compd. 2020;819:153008.
- [135] Cui Z, Li W, Cheng L, et al. Effect of nano-HA content on the mechanical properties, degradation and biocompatible behavior of Mg-Zn/HA composite prepared by spark plasma sintering. Mater Charact. 2019;151:620-631.
- [136] Dvorsky D, Kubasek J, Jablonska E, et al. Mechanical, corrosion and biological properties of advanced biodegradable Mg-MgF2 and WE43-MgF2 composite materials prepared by spark plasma sintering. J Alloys Compd. 2020;825:154016.
- [137] Singh B, Singh R, Mehta JS, et al. Nano-mechanical characterization of Mg-Zn-Mn-Si alloy fabricated by spark plasma sintering for biomedical applications. Mater Today Proc. 2018;5:27742-27748.
- [138] Cui Z, Zhang Y, Cheng Y, et al. Microstructure, mechanical, corrosion properties and cytotoxicity of beta-calcium polyphosphate reinforced ZK61 magnesium alloy composite by spark plasma sintering. Mater Sci Eng C. 2019;99:1035-1047.
- [139] Soderlind J, Cihova M, Schäublin R, et al. Towards refining microstructures of biodegradable magnesium alloy WE43 by spark plasma sintering. Acta Biomater. 2019;98:67-80.
- [140] Cao NQ, Pham DN, Kai N, et al. In vitro corrosion properties of Mg matrix in situ composites fabricated by spark plasma sintering. Metals. 2017;7:358.
- [141] Ghasali E, Bordbar-Khiabani A, Alizadeh M, et al. Corrosion behavior and in-vitro bioactivity of porous Mg/Al₂O₃ and Mg/Si₃N₄ metal matrix composites fabricated using microwave sintering process. Mater Chem Phys. 2019;225:331-339.
- [142] Vanmeensel K, Laptev A, Hennicke J, et al. Modelling of the temperature distribution during field assisted sintering. Acta Mater. 2005;53:4379-4388.
- [143] Olevsky EA, Bradbury WL, Haines CD, et al. Fundamental aspects of spark plasma sintering: I. Experimental analysis of scalability. J Am Ceram Soc. 2012;95:2406-2413.
- [144] Olevsky EA, Garcia-Cardona C, Bradbury WL, et al. Fundamental aspects of spark plasma sintering: II. Finite element analysis of scalability. J Am Ceram Soc. 2012;95:2414-2422.
- [145] Tokita M. The potential of spark plasma sintering (SPS) method for the fabrication on an industrial



- scale of functionally graded materials. Adv Sci Technol. 2010;63:322-331.
- [146] Manière C, Torresani E, Olevsky EA. Simultaneous spark plasma sintering of multiple complex shapes. Materials. 2019;12:557.
- [147] Musa C, Licheri R, Locci AM, et al. Energy efficiency during conventional and novel sintering processes: the case of Ti-Al₂O₃-TiC composites. J Cleaner Prod. 2009;17:877-882.
- [148] Kelly JP, Graeve OA. Spark plasma sintering as an approach to manufacture bulk materials: feasibility and cost savings. JOM. 2015;67:29-33.
- [149] Tokita M. Spark plasma sintering: method, systems, applications and industrialisation. Powder Metall Rev. 2019;8:89-102.
- [150] Manière C, Zahrah T, Olevsky EA. Inherent heating instability of direct microwave sintering process: sample analysis for porous 3Y-ZrO2. Scr Mater. 2017;128:49-52.
- [151] Manière C, Zahrah T, Olevsky EA. Fully coupled electromagnetic-thermal-mechanical comparative simulation of direct vs hybrid microwave sintering of 3Y-ZrO₂. J Am Ceram Soc. 2017;100:2439-2450.